8-2022

An economical and repeatable method for mapping shade cast on water channels

Eric M. Nielsen
Portland State University, emn2@pdx.edu

An economical and repeatable method for mapping shade cast on water channels

Eric M. Nielsen*
Institute for Natural Resources, Portland State University
August 2022

1. Introduction

1.1. Overview

The motivation of this work is to provide insights toward determining a viable strategy for statewide monitoring of riparian vegetation condition, with particular focus on developing a repeatable, cost-effective method for assessment of progress toward achieving temperature-based water quality standards mandated by the federal Clean Water Act. A reliable monitoring strategy could in turn support a data-driven prioritization and assessment framework to increase the efficiency, effectiveness and accountability of riparian restoration efforts. In this project we developed and tested a method for mapping shade cast on water channels by riparian vegetation using optical imagery sources that are affordable and regularly available across the state of Oregon.[1] We validated the optical imagery-based results against lidar-based shade estimates that—while superior for the application—do not represent a viable approach for ongoing statewide monitoring due to their expense.

The optical imagery sources we evaluated were 1-foot resolution aerial imagery from the National Agricultural Imagery Program (NAIP) and 10-meter resolution Sentinel-2 satellite imagery. The model results were assessed by comparing them to shade estimated using solar-path modeling applied to lidar data collected over three study areas spanning a wide range of environmental conditions. The optical-based results explain nearly 77% of the variation in lidar-derived shade across the study areas. NAIP-based models significantly outperformed Sentinel-2 models; we found that multi-scale image textural information derived from NAIP was important in creating accurate shade estimates. Maps of shade from the optical-based model were created over the entire Johnson Creek watershed in metropolitan Portland; visual inspection of the results shows a very high correspondence to photo-interpreted NAIP imagery, including accurate response to subtle and fine-scale variation in conditions.

This report describes the methods we used to create and assess the optical-based shade map, shares the results of the assessment, and provides the modeled output over the Johnson Creek watershed. It also describes a sample design and field protocol that were created to support a field effort to provide additional validation of the approach. The field effort has not yet been performed, but perhaps is not necessary due to the seeming reliability of lidar data as a validation data source.

1.2. Strategy

Model construction and validation were originally planned to occur in two phases. First, field shade estimates from Solar Pathfinder and/or hemispherical photography were to be used to validate a shade model based on gridded lidar data. This model would allow shade mapping within spatial and temporal constraints determined by lidar data availability. Second, the lidar shade model was to be used as a bridge

* Correspondence: emn2@pdx.edu.

[1] The primary imagery sources with these characteristics and of sufficient resolution for the task are aerial imagery from the National Agricultural Imagery Program (NAIP) and satellite imagery from the Sentinel-2 sensors. Since these are optical imagery data sources, we refer to them hereafter as "optical imagery."

for development and validation of a shade model based on optical imagery. This second model would provide the capability for wall-to-wall shade mapping across the state, with the capacity to be updated when new cloud-free imagery is obtained (ideally annually).

The fieldwork planned by Oregon Department of Environmental Quality (ODEQ) that would validate the first modeling phase did not go forward as planned. The results we present here are therefore limited to an assessment of the second phase, the validation of optical imagery-based shade maps against lidar-supported solar modeling. Despite the omission of the ground-truth component, cast shade estimates based on lidar imagery have been found to be essentially equivalent to onsite measurements (e.g., National Renewable Energy Laboratory 2015). The validation of the optical imagery model presented here is very likely to be functionally complete.[2]

1.3. Study area

Three pilot areas were selected for analysis (Figure 1); each of the three contains temperature-priority watersheds (TPW) recognized by ODEQ. Collectively, these watersheds include a wide variety of climatic conditions (e.g., maritime, inland valleys, high elevation Cascades, and semi-arid east slope Cascades) and land use types (e.g., industrial timberland, natural conifer and broadleaf forests, mesic and dryland agriculture, and urbanized). The watersheds were selected to permit cost-effective field sampling by ODEQ crews. Though they incorporate a broad range of conditions, they are not as representative of non-forest land found in more arid regions farther east in Oregon, although the lower portion of the East Cascades area has some characteristics in common with that.

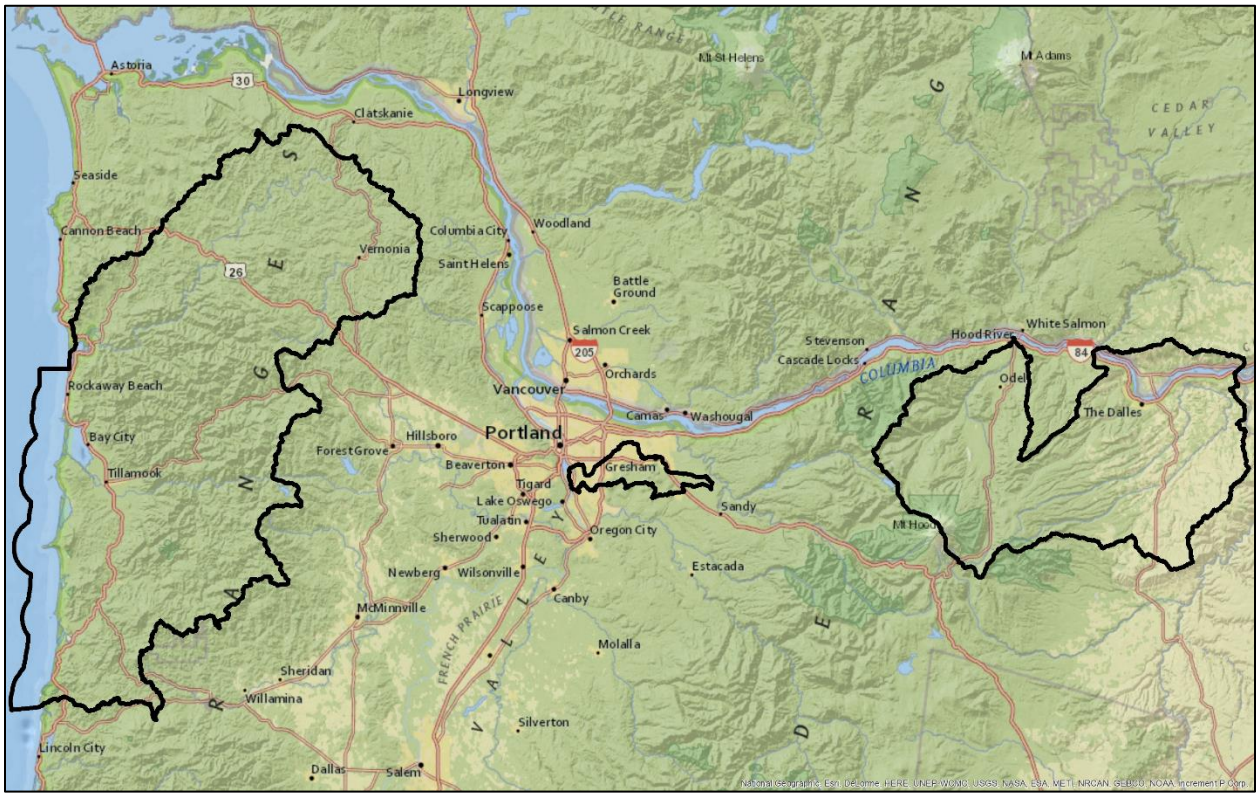

Figure 1. Pilot watersheds. From west to east, we refer to these areas as (1) Coast Range, including the North Coast Sub-basins & Wilson-Trask-Nestucca TPWs; (2) Johnson Creek, including the Lower Willamette Sub-basin TPW; and (3) East Cascades, including the Miles Creeks & Western Hood TPWs.

[2] Although information pertaining to the field sample design and protocol is not relevant to the results presented here, we have included it to support possible future ground-truth efforts.

2. Methods

All analysis steps below were performed in Python 2.7 (mostly using the arcpy library) or in R 4.0.2.

2.1. Image data processing

All available lidar data within the pilot areas were acquired from the Oregon Lidar Consortium (Oregon Department of Geology & Mineral Industries 2021). The 22 lidar datasets that included both bare earth and highest hit elevation layers and appeared to consist of reliable data were processed on a by-quad basis to a common horizontal resolution (one meter) and vertical unit (quarter-foot) before calculating canopy height as the difference between highest hit and bare earth elevations. We then reprojected the quad data to Zone 10 UTM using the NAD83 horizontal datum, resampled all layers to 3-meter resolution to ease the subsequent processing burden, and mosaicked them across each of the pilot watersheds. The year of each collection was extracted and similarly mosaicked across the watersheds. Lidar collection years ranged from 2009 to 2015.

1-foot resolution 4-band aerial imagery collected in 2018 was acquired from the Oregon Imagery FIT program (Oregon Geospatial Enterprise Office 2021), and nested texture metrics were produced across the pilot areas (see Nielsen et al. 2021 for a description of this algorithm, created at INR). The resulting metrics were summarized at 10-foot resolution over both the local pixel and over a 130-foot square moving window in which each the contribution of each pixel in the south half of the window was weighted proportionally to its inverse-distance from the center pixel and to the cosine of the angle between it and the center pixel (in order to represent the potential shade cast on the center pixel by vegetation at each nearby pixel).

Sentinel-2 satellite reflectance data was obtained using Google Earth Engine (Google 2021). A medioid mosaic method was used to remove clouds, cloud shadows and other corrupt data from all Sentinel-2 images collected over the pilot areas between July 1, 2020 and September 1, 2020. The red, green, blue, near-infrared and two shortwave infrared bands were obtained in this way at their native 10-meter or 20-meter resolution. All data were resampled to 10-meter resolution using a cubic convolution resampling method. A variety of spectral indices were created from the reflectance data; the metrics are reviewed in Nielsen et al. (2021). Like the NAIP metrics, these metrics were summarized both at the local pixel and over an inverse-distance moving window oriented toward the south.

Historic image data was needed to assess change across the study area since the date of lidar collection. Landsat 5 and Landsat 8 satellite reflectance data was obtained for 2020 and for every year in which any of the lidar collections had been obtained (2009, 2010, 213, 2014, 2015). Google Earth Engine was used to create a medioid mosaic from imagery collected between July 1 and September 1 of each year. The red, green, blue, near-infrared and two shortwave infrared bands were obtained at their native 30-meter resolution.

2.2. Derived lidar metrics

2.2.1. Hydrologic flow paths

We derived flow paths and a channel network from the lidar data, to serve as a check on the NHD channel delineation and to provide reference locations likely to be on channels for use in the field sample selection to be performed by ODEQ. We first aggregated the lidar bare earth mosaic to 3-meter resolution, a tractable but sufficient resolution to support flow modeling. We aggregated using a moving window minimum function, to preserve local minimum elevations most likely to represent the exact location of channels. We then used the built-in ESRI hydrologic functions to fill sinks and calculate local flow direction and accumulation. With reference to Strahler orders from the NHD over coincident channel reaches, we estimated minimum flow accumulation breakpoints corresponding to Strahler orders 1, 3, 5 and 7, and created a 3-meter resolution raster representing the distribution of these channel orders over the study area.

2.2.2. Solar modeling

We used the ArcGIS solar modeling tools (ESRI 2021) to produce solar radiation estimates along channels throughout the study area. These tools allow the user to provide a set of points and an elevation surface, and calculate the cumulative solar radiation on each point across a selected time window, incorporating the shade cast by a surrounding elevation surface.[3] By using the highest hit elevation resampled to 3-meter resolution as the surface, the impact of surrounding vegetation on incoming radiation can be estimated. However, because the thermal load at a given location requires an estimate of radiation impacting the ground surface, regardless of the height of the vegetation present above it, the surface provided must have the bare earth elevation substituted for the highest hit elevation at each provided point where radiation is to be estimated, while using the highest hit elevation to represent the vegetation present at all surrounding pixels.

We accomplished this in two steps, computed separately so as to avoid interfering with each other. In the first run, direct radiation impacting NHD channels was estimated by running the solar modeling tool on a set of points centered on each 3-meter pixel along all NHD channels, using an elevation raster containing the bare earth elevation for the NHD channel pixels but the highest hit elevation value at all other pixels. This allowed an estimate of radiation on NHD channel locations, assuming that relatively little shade is cast along the direction of the channel itself (this assumption is violated only along extended north-south running channel reaches, and even there, the fine analysis resolution reduces the impact to manageable levels). A second direct radiation run was conducted for the flow paths designated in the lidar-based hydrological analysis. In this case, the bare earth elevation was substituted for the highest hit elevation only along the delineated flow paths. The results from the two analyses were converted from point vector to raster format and merged into a single raster. In order to separate the shade cast by vegetation from that cast by surrounding terrain, an additional direct radiation run was conducted using the bare earth elevation at all pixels. We created a metric called "shading fraction" to represent the solar radiation impacting the channel surface *relative to the radiation that would reach the surface if there were no surrounding vegetation*:

$$SF = 1 - \frac{DR_{HH}}{DR_{BE}}$$

where SF is the shading fraction, DR_{HH} is the direct radiation incorporating shade cast by the surrounding highest hit elevation values, and DR_{BE} is the direct radiation incorporating shade cast only by the surrounding bare earth elevation values. If SF is near 1, the vegetation is blocking most of the radiation that makes it past the surrounding terrain alone; in other words, the vegetation is effectively shading the channel. If SF is near 0, the radiation reaching the surface in the presence of surrounding vegetation is nearly as high as that reaching based on terrain alone; in other words, surrounding vegetation is contributing little toward shading the channel in excess of the shade cast by terrain alone. We use SF here as a practical representation of the performance of vegetation in contributing shade at any location. However, note that it would not be the best measure for, e.g., identifying "hot spots" along the entire length of a stream, because surrounding terrain may provide significant shade in some cases. in this case, DR_{HH} would be more appropriate. The two quantities are highly related; if anything, DR_{HH} is easier to map, especially from optical imagery.

[3] We used the total direct radiation cast on the non-leap year days April 22, May 22, June 21, July 21, August 20 and September 19 to create an estimate approximately proportional to the total radiation through the warmer months of the year. Radiation was modeled every 15 minutes on each of these days.

2.3. Landsat change analysis

Because much of the lidar data available is fairly old, it was necessary to filter out locations that had changed significantly since its collection. Removing changed areas from the sample draws for field sampling and model training greatly improves the chances that field sample locations represent the current conditions they are intended to (see sample stratification below), and that model training samples represent similar conditions in the lidar training data, the 2018 aerial imagery, and the 2020 satellite imagery.

We used a Landsat-based change detection method to find areas where land cover had changed substantially between the lidar acquisition and 2020. We began by creating a composite of historic Landsat 5 imagery, choosing which year to draw each pixel's reflectance data from based on the year the lidar data at that location was collected. We then created a change image by subtracting the historic reflectance data from the 2020 Landsat reflectance data. To flag changed areas, we used the ArcGIS Iso-Cluster Unsupervised Classification function to create 50 distinct spectral clusters from the change image. Each of the 50 clusters was manually assigned to represent either change or no-change based on visual inspection of the historic and current imagery. Changed areas—which were primarily associated with logging and reforestation, development, and agricultural transitions—were eliminated from consideration for selection of field or training samples in the steps below.

2.4. Sample design

The sample design involved three main steps: formation of sampling strata along channels in the study area, determination of accessibility masks from which samples were drawn, and stratified random selection of sites from each strata within the accessibility masks.

2.4.1. Sample stratification

The sample design attempted to steer field sampling toward a range of sites sufficient to support the construction of models to estimate shade based on independent variables that can be produced wall-to-wall across the state. The variables included in the stratification are as follows:

A. Surrounding land cover type, based on dominant National Land Cover Dataset (NLCD) class in the surrounding four-hectare area, grouped into (1) conifer forest, (2) broadleaf-mixed forest, (3) agriculture, (4) human-developed, and (5) non-forest (often post-logging or otherwise disturbed). ***Justification:*** The accuracy with which shade can be mapped from lidar or from image-based variables will likely vary between different land cover types along with changes in the dominant components of ground, shrub and tree layer vegetation and in the spatial scales at which they are distributed. The confounding factors impacting the ability to map accurately also may be land cover dependent. The image-based variables that are important for estimating shade also likely vary between land cover types, so it's important to make sure models are trained on all of them.
B. Average precipitation of the months of January, April, July and October, based on PRISM climate normals (PRISM Climate Group 2021). The five land cover types above were split into ten landscape types using natural breaks in precipitation corresponding to distinct environments. Resulting types were dry (east-side) conifer (< 90 mm average), mesic conifer (90-150 mm), wet conifer (higher elevations, especially in the coast range, > 150 mm), dry-mesic broadleaf forest (< 150 mm), wet broadleaf forest (coast range, > 150 mm), dryland agriculture (Hood River and The Dalles, < 80 mm), mesic agriculture (> 80 mm), developed, dry non-forest (east-side woodlands, shrublands and herbaceous, < 65 mm) and mesic-wet non-forest (mostly logging disturbance, > 65 mm). ***Justification:*** Gridded lidar data only provides information on canopy height and isn't aware of the vertical distribution of canopy. Optical imagery also has little sensitivity to this. Although we cannot stratify based on the vertical distribution of canopy *per se*, annual

precipitation can serve as a proxy variable for shifts in species composition across the pilot project area (from trees with foliage extending well below the canopy top, e.g. western hemlock and western red cedar, in the west, to trees with top-heavy foliage distributions, e.g., ponderosa pine, in the east).[4]

C. NHD channel Strahler order, categorized into small (order 1–2, typically without significant break in canopy overhead), medium-small (order 3, often with canopy break), medium-large (order 4, usually with canopy break) and large (order 5–7, always with canopy break) channels. Intersecting the four channel size categories with the ten landscape types above yielded 40 classes. ***Justification:*** Variation in channel size is associated with changes in vegetation structure, on the capability of streamside vegetation to provide shade to channels, and in additional covariates (e.g., local slope) that can impact the relationship between remotely sensed image data and effective shade.

D. Shading fraction, defined as $1 - \frac{R_{HH}}{R_{BE}}$, where R_{HH} represents midsummer direct solar radiation as estimated using ArcGIS solar radiation tools parameterized with 3-meter resolution vegetation highest hit elevation data,[5] and R_{BE} represents midsummer direct solar radiation parameterized with bare earth elevation. Variation in the intensity of insolation resulting from interaction of the local slope and aspect and solar angle was not considered in either of these calculations, because this quantity can be easily estimated with a simple physical model. Each of the 40 classes resulting from the previous step were broken into four shading fraction quartiles with equal number of pixels. ***Justification:*** Effective shade is the primary variable we are attempting to map; stratification is important to ensure accurate estimation across its range.

E. Average vegetation height within a 15-meter radius semicircle between 90° and 270° from the sample location. This variable integrates both dominant canopy height and canopy cover. Abundant classes with a particularly wide range of vegetation heights were divided into tall and short vegetation variants by splitting them at the median vegetation height for the class. 40 of the 160 classes resulting from the previous step were split, resulting in a total of 200 sample strata. ***Justification:*** Different vegetation types, canopy structures, and distance from sample location may result in the same shading fraction. Stratifying based on this variable ensures a sample that incorporates these distinct variants.

2.4.2. Accessibility mask

Sample sites were chosen along channels represented in the NHD, geographically limited to accessible regions. We considered two strategies for representing accessibility. The first strategy is informed by the known locations where ODEQ field sampling has occurred in the past. These stations lie along a variety of channel sizes in each of the pilot watersheds. Sample sites within 100 meters of the stations—along the same channel reach that was visited previously—are likely accessible. The second strategy limits sampling to sites on public land (within the pilot areas, mostly within the Tillamook and Clatsop State Forests, the Mount Hood National Forest, and on Bureau of Land Management land, along with various chunks of land managed by various state and local entities). These sites are subject to the following additional limiting criteria: (a) within 20–120 meters of a road that is (b) no more than 10 road kilometers distant from a ODOT-managed highway or ODEQ station and (c) reachable on foot by traversing a limited cost distance in which travel across areas of over 30° slope is penalized and travel across areas of over 45° slope is prohibited.

[4] Coniferous and broadleaf forests also will vary in this regard. This is accounted for by the land cover stratification variable.

[5] In this calculation, 3-meter pixels along stream channels—as represented by NHD—were assigned the local bare earth (terrain) lidar elevation, while all other pixels were assigned the local highest hit (surface) elevation.

We assessed the representativeness of the two accessibility masks with respect to the overall landscapes traversed by channels within the pilot watersheds. We represented the overall riparian landscape by buffering all channels by 20 meters, and the accessible riparian landscapes by buffering the two accessibility masks by 20 meters. We then summarized and compared the accessible landscapes to the overall landscape with respect to the distribution of several key variables (see Appendix A). We found that while the public lands mask generally represented the overall riparian landscape faithfully, the stations-based mask differed in several key aspects. Areas with vegetation less than one foot in height, at very low elevations, with very low slopes, and containing agriculture, development and roads were all substantially over-represented near stations. Higher slopes adjacent to channels, upper elevations, and conifer forests were all very poorly represented there. Stations were also biased toward medium to large channel sizes, although this did not in itself represent an unsurmountable challenge. The single deficiency in the public lands mask was in its poor representation of the lowest precipitation area within the pilot watersheds, the lower elevations of the 'Miles' creeks above The Dalles.

2.4.3. Sample selection

Because points were drawn from the combined accessibility masks, and the area represented in the public lands mask was nearly eight times that represented in the station-based mask, it is likely that the majority of potential targets for most strata lie within the public lands mask rather than the station-based mask. Although these sites may be somewhat more difficult to reach, they provide a much less biased representation of conditions on riparian areas in the study area.

ODEQ estimated that they would have resources and time available to collect approximately 200 field plots. Therefore, we set a goal of one plot collected from each of the 200 strata. ODEQ agreed to review target locations in the office in advance of fieldwork, in order to verify that the selected plots were likely reachable in the field. INR supported this plan by producing twenty randomly chosen potential sample targets from each of the 200 strata, and by providing ODEQ with a simple methodology for selecting a single target for each. For each strata, if the first potential sample target did not appear accessible—due to land ownership, area closures, road access issues, or other obstacles—the ODEQ analyst would reject that target and proceed to examine subsequent potential targets.

2.5. Field protocol

INR developed a field protocol for use in gathering data for validation of the lidar-based shade estimates. Multiple, spatially distributed estimates of shade are needed in order to reduce field sample estimation error and properly validate the lidar-based model, particularly on larger channels where variability in shade might be encountered across the channel.

2.5.1. Basic instructions

The field procedure proposed by INR is summarized here. The fieldsheet (Appendix B) includes additional instructions.

A. Upon arrival at GPS target location, navigate to the nearest bank of a channel matching the target channel size.
B. Measure azimuth of stream flow and estimate bank to bank channel width perpendicular to flow.
C. Estimate slope and aspect of land at 20-meter scale, looking away from channel from each bank point.
D. Establish hemispherical photo point (HPP) on the southernmost bank of the channel, if accessible (this instruction is contingent on ODEQ's report that collecting a photo in the channel center would be difficult). If southernmost bank is not accessible, establish photo point on the accessible bank. Document photo point location via averaged GPS, plot diagram, cardinal direction photos, and laser-

measured distance and azimuth with respect to true north to witness locations (prominent features such as manmade objects, easily identifiable trees etc.).

E. Collect five Solar Pathfinder shade estimates. The first should be at the same location as the HPP, the 2nd should be at 25% of the way across the channel, the 3rd at 50%, the 4th at 75%, and the 5th should be at the opposite bank.
F. Complete reference and patch diagrams (see fieldsheet, Appendix B). Areas of relatively homogeneous vegetation or land cover should be described as separate patches. Among other purposes, the diagrams will be used for later quality control of the plot location, with reference to aerial imagery.
G. Collect vegetation cover and height data in a half-circle of 20-meter radius centered on the HPP and oriented in a southerly direction. Note whether lidar data appears valid, estimate percent canopy cover within vegetation categories (see fieldsheet), and use laser to measure height of tallest vegetation and of dominant veg layer.
H. Collect vegetation cover and height data of vegetation overlapping the channel in a 10-meter wide band perpendicular to the channel.
I. If doable quickly and with confidence, identify up to three dominant species within each vegetation category.

2.5.2. Vegetation/land cover categories

We developed the following vegetation and land cover categories for use in describing the vegetation present in each distinct patch at the field site. We distinguish conifers and broadleaved trees from shrubs by specifying that they must regularly attain greater than 20 feet height at maturity. Broadleaved trees in our area include red alder, black cottonwood, bigleaf maple, vine maple, Pacific madrone, etc.

B1: Broadleaf trees, < 5 feet tall
B2: Broadleaf trees, 5–20 feet tall
B3: Broadleaf trees, 20–80 feet tall
B4: Broadleaf trees, 80+ feet tall
C1: Conifers, < 5 feet tall
C2: Conifers, 5–20 feet tall
C3: Conifers, 20–80 feet tall
C4: Conifers, 80+ feet tall
S1: Shrubs, < 5 feet tall
S2: Shrubs, 5+ feet tall
H: Herbaceous vascular vegetation (including forbs, grasses, sedges, rushes and ferns)
A: Aquatic vegetation
U: Unvegetated areas
W: Water

2.6. Optical imagery-based shade mapping

2.6.1. Training data

The 3-meter resolution lidar-based shading fraction dataset was resampled to 10-foot resolution to match the NAIP-based image data, and 3000 training samples were drawn from it. 300 training samples were randomly selected from each of the ten landscape types created based on land cover and precipitation (see section 4.4.1 #2, above). Shading fraction data were selected only from the lidar-generated flow paths, to ensure that the capabilities for optical-based shade mapping were tested on channels rather than in the more haphazard NHD locations.

2.6.2. Predictor data

In addition to the metrics created from NAIP and Sentinel-2 imagery (described in section 4.1), we generated a suite of predictors describing topographic setting and local climate normals. The topographic metrics were created from the bare earth lidar data[6] across the study area, and the climate normals were extracted from the PRISM data. Nielsen et al. (2021) contains a review of the topographic and climate metrics used. The Sentinel-2, topographic, and climate metrics were resampled to 10-foot resolution to match the NAIP-based metrics.

2.6.3. Modeling

We used the R language implementation of random forest (RF) regression modeling (Liaw and Wiener 2002) to create a model to predict shading fraction from NAIP imagery, Sentinel-2 imagery, and topographic and climate metrics. An original predictor selection algorithm, described in Nielsen et al. (2021), was used to simultaneously optimize model accuracy and model effective resolution. The optimal predictor set was chosen by minimized the sum of out-of-bag root mean square error (RMSE) and mean absolute error (MAE). The selected predictors were then used to create a RF regression model of 501 trees. Out-of-bag model statistics were extracted, allowing model error assessment either cumulatively or across any subset of training plots. We used reduced major axis (RMA) regression to compensate for model bias toward the mean at the lowest and highest values of shading fraction (see Belitz and Stackelberg 2021). The model was then predicted wall-to-wall at 10-foot resolution across the Johnson Creek pilot area to provide an example of an effective shade map produced from optical imagery with no lidar data available.

3. Results

3.1. Lidar-based shade map from solar modeling

Shading fraction, calculated from lidar data as described in section 4.2.2., was mapped across the pilot areas for all NHD channels and lidar-derived flow paths. The results appeared very plausible. A small excerpt of the layer, in Portland's Johnson Creek watershed, is shown in Figures 2 and 3.

[6] Note that although the topographic metrics were created from lidar bare earth layers, the metrics used could also have been created from standard USGS digital elevation models. The resulting model is applicable to a use case where lidar data is not available.

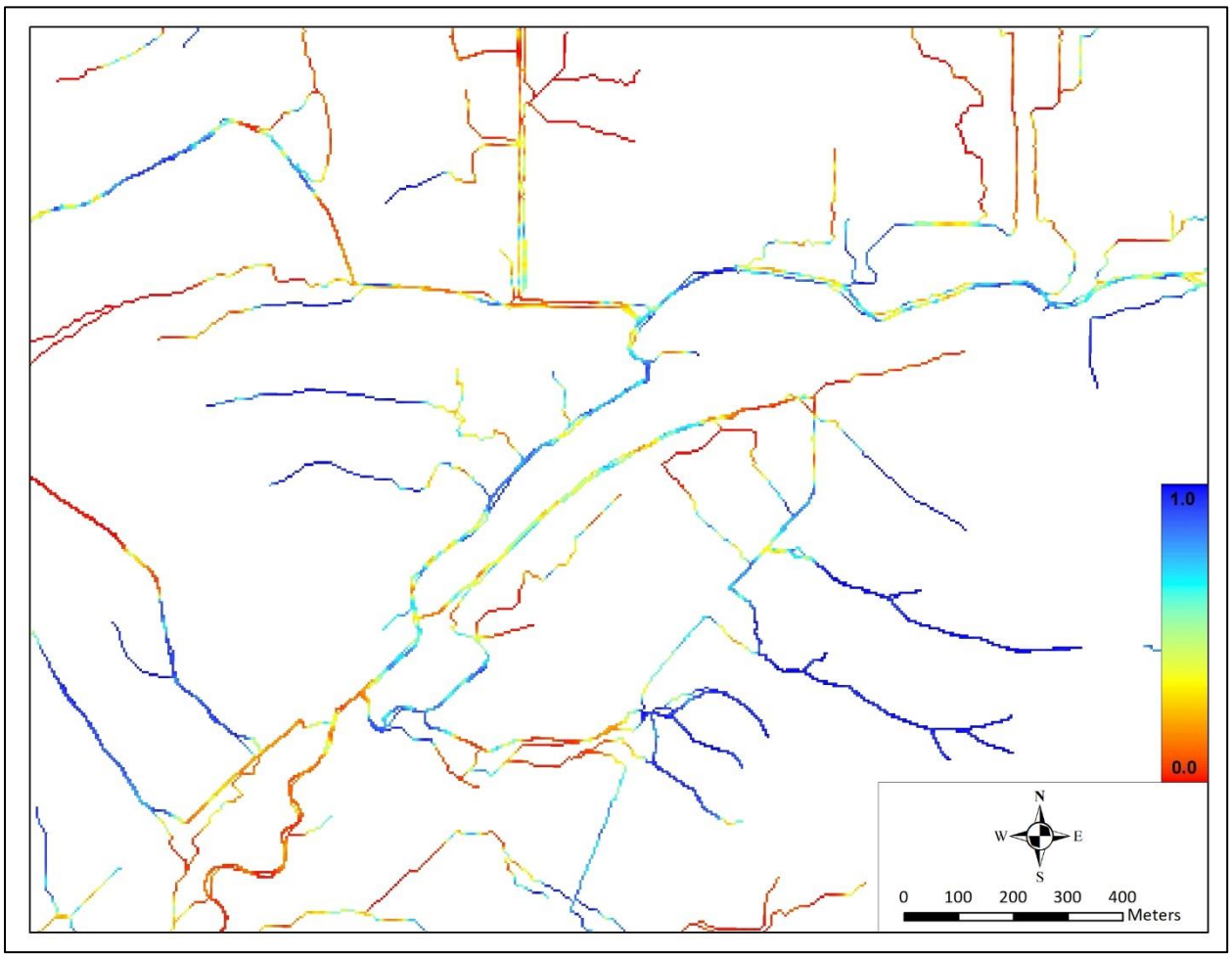

Figure 2. Shading fraction generated from lidar-based solar modeling, along and near Johnson Creek just southeast of Powell Butte in Portland. Values range from 0 (no shade provided by vegetation, dark red) to 1 (complete shade provided by vegetation, dark blue).

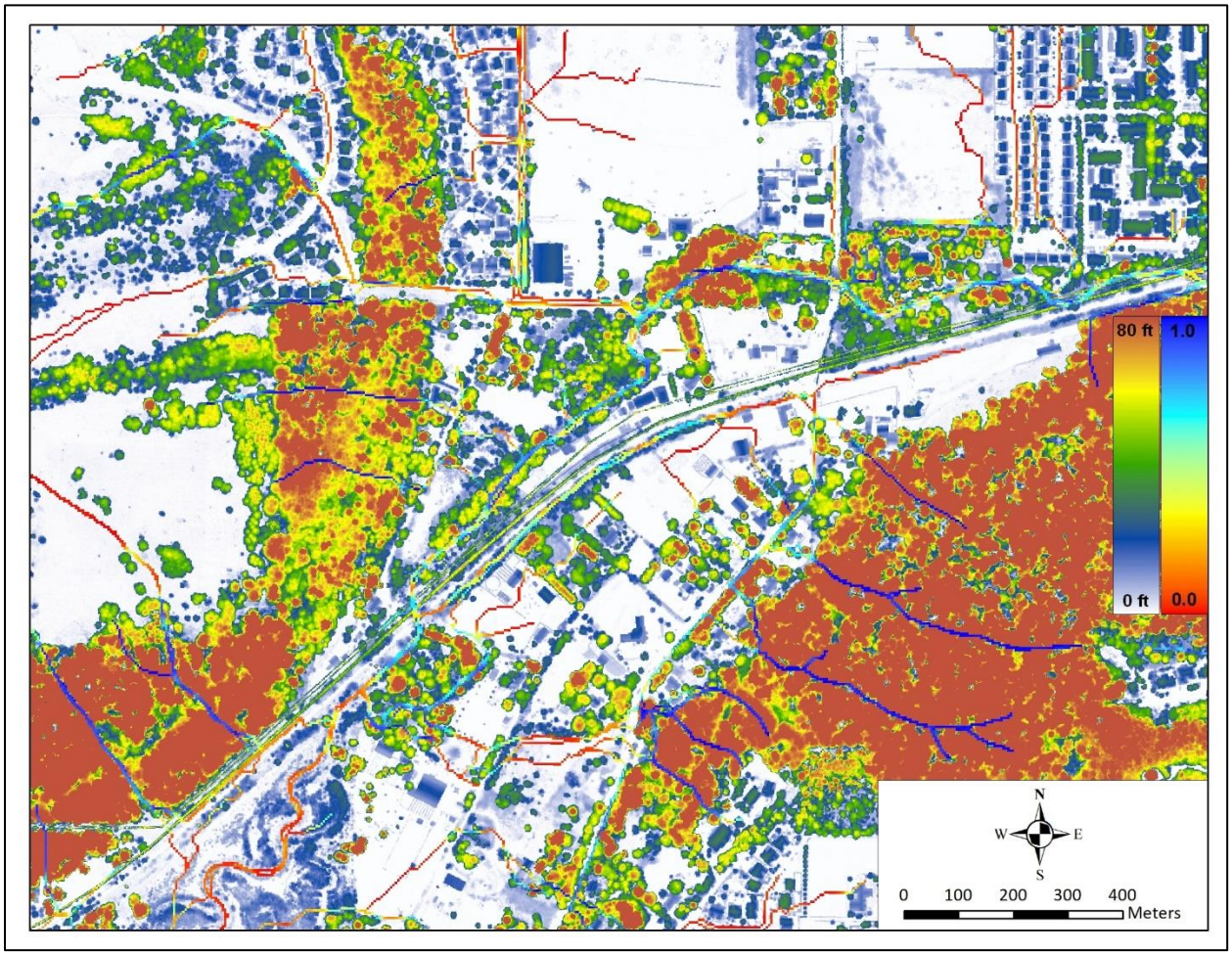

Figure 3. Shading fraction as in Figure 2, superimposed on lidar-based vegetation height. Height color ramps from white (zero), through blue (~20 feet), green (~40 feet), yellow (~60 feet) to red (80 feet plus).

3.2. Optical imagery-based shade map

3.2.1. Selected predictors and predictor importance

The selected predictors and their relative importance values, which are proportional to the increase in model mean square prediction error in runs excluding them, are shown in Table 1.

Predictor name	Description	Relative importance
m_u1_md	NAIP median near-IR:green contrast, over south-facing shade window	1.000
s_grn	Sentinel-2 green reflectance, local	0.630
n_gcb	NAIP green band 12′ res center pixel vs 8NN median, local	0.233
m_wa_13	NAIP green:red contrast standard deviation NDTI, 1′ vs 3′ res, over south-facing shade window	0.177
m_u4b	NAIP near-IR:green contrast 4′ res center pixel vs 8NN median, over south-facing shade window	0.161
t_rough90	topographic roughness at 90-meter scale	0.135
n_y1_mx	NAIP maximum red:blue contrast, local	0.110
n_wa_26	NAIP green:red contrast standard deviation NDTI, 2′ vs 6′ res, local	0.104
m_w2b	NAIP green:red contrast 2′ res center pixel vs 8NN median, over south-facing shade window	0.099

m_gb_4c	NAIP green band center pixel vs 8NN median NDTI, 4′ vs 12′ res, over south-facing shade window	0.083
p_ppt_oct	average October precipitation	0.078
m_ub_26	NAIP near-IR:green contrast center pixel vs 8NN median NDTI, 2′ vs 6′ res, over south-facing shade window	0.071
t_hl3	topographic heat load at 3-meter scale	0.064
t_be3m	elevation	0.062
m_ga_13	NAIP green band standard deviation NDTI, 1′ vs 3′ res, over south-facing shade window	0.058
s_ndnbp	Sentinel-2 near-IR:blue contrast, local	0.049
n_u1b	NAIP near-IR:green contrast 1′ res center pixel vs 8NN median, local	0.047
n_g4a	NAIP green band 4′ res standard deviation, local	0.043
z_ndgbp	Sentinel-2 green:blue contrast, over south-facing shade window	0.038
m_gb_13	NAIP green band center pixel vs 8NN median NDTI, 1′ vs 3′ res, over south-facing shade window	0.037
z_ndswp	Sentinel-2 shortwave bands contrast, over south-facing shade window	0.035
z_ndsip	Sentinel-2 red:mid-IR contrast, over south-facing shade window	0.031
n_n1_mx	NAIP maximum near-IR band, local	0.019
n_ub_13	NAIP near-IR:green contrast center pixel vs 8NN median NDTI, 1′ vs 3′ res, local	0.010

Table 1. Selected predictors and relative importance values. Additional information about the terms used in the table can be found in Nielsen et al. (2021).

The predictor importance values, totaled by the data source they were derived from, are shown in Table 2. Aerial imagery from NAIP is clearly the most informative overall data source. Sentinel-2 imagery and topography provided some additional predictive power when added to the NAIP-based information.

Predictor source	Relative importance
NAIP	1.000
Sentinel-2	0.348
Topography	0.116
Climate	0.035

Table 2. Total relative importance of predictors by data source.

3.2.2. Model accuracy

The resulting model for shading fraction based on optical imagery, topography, and climate data had an R^2 of 0.7668. In other words, 76.68% of the variability in shading fraction computed from solar modeling using lidar data can be explained without reference to lidar data. The root mean square error (RMSE) and mean absolute error (MAE) of the model were 0.1941 and 0.1339 respectively.[7] All model accuracy rates were estimated over bootstrap-aggregated samples, totally independent from the test data. The estimates were made using the same number of trees that were used for the actual predictions. Multiple studies have found that RF avoids overfitting to training data (e.g., see Fox et al. 2017) and that model accuracy estimates made in this way tend to be conservative.

[7] Values of the predicted variable, shading fraction, ranged from 0 – 1.

3.2.3. Bias correction

The shading fraction test values and the corresponding raw out-of-bag predictions were used to create the density plot shown in **Figure 4**. Note the strongly bimodal nature of effective shade; many sites are either nearly fully shaded or mostly exposed to sun. The deviation from a 1:1 line resulting from over-prediction of low values and under-prediction of high values is typical of machine learning regression modeling and can be reduced in several ways (Zhang and Lu 2011). We used RMA regression (the regression line labeled "RMA" in Figure 4) to match the mean and variance of predicted shading fraction to the test dataset. The bias-corrected predictions are shown against the test values in Figure 5. Note that the RMA regression line in Figure 5 lies very near the desired 1:1 relationship.

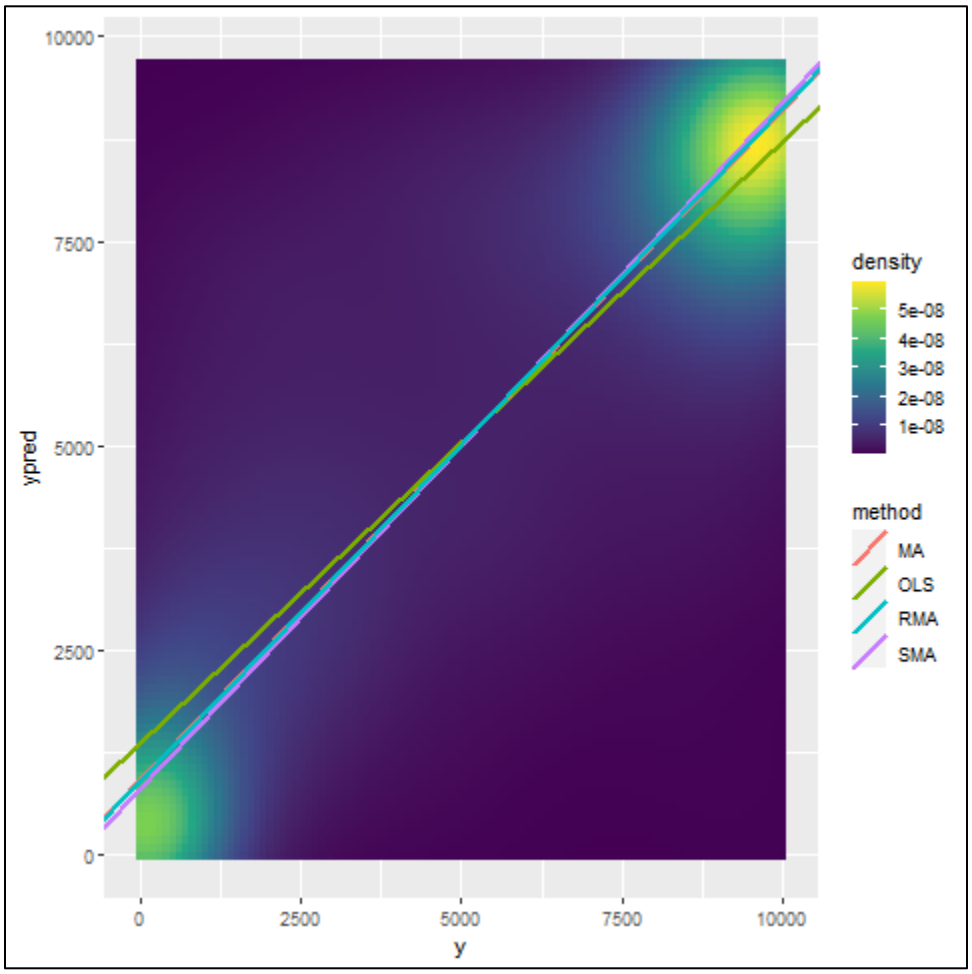

Figure 4. Density plot of shading fraction test values (x axis) and corresponding predictions (y axis), with several best-fit regression lines computed by various methods. Shading fraction, whose real values range from 0 – 1, is scaled up by a factor of 10,000 here.

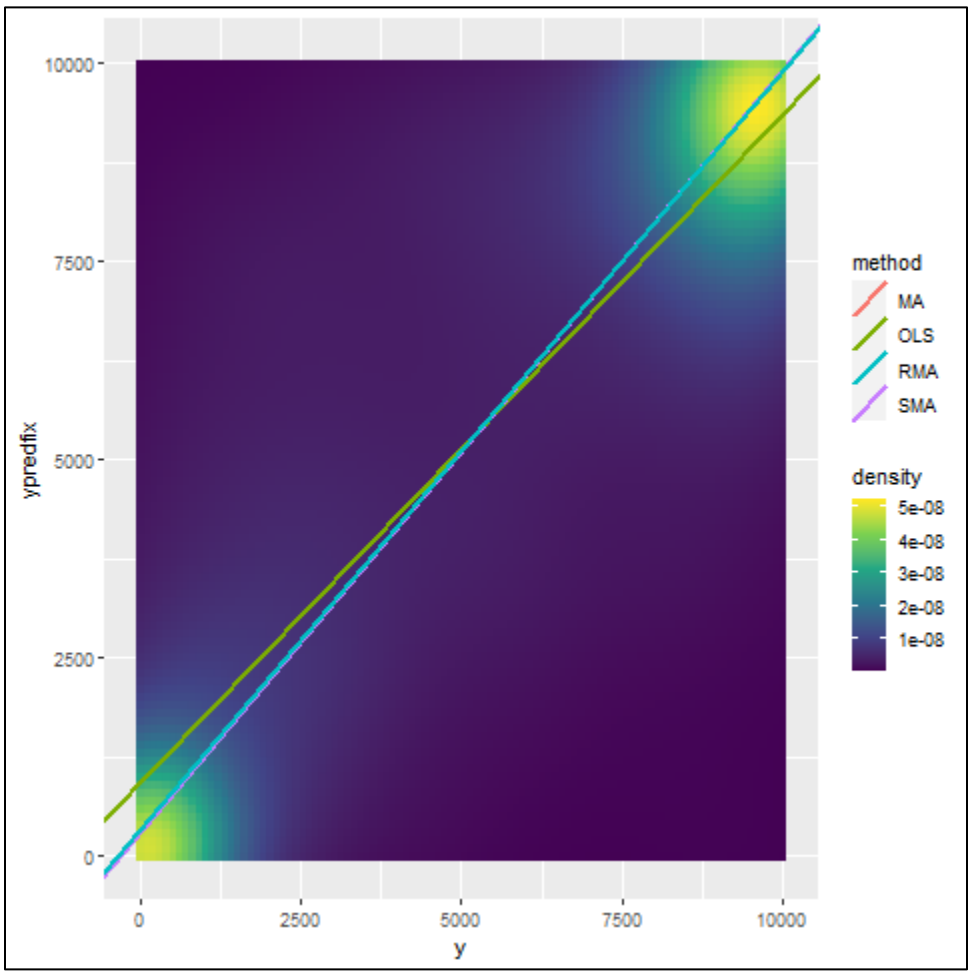

Figure 5. Density plot of test values (x axis) and bias-corrected predictions (y axis).

3.2.4. Maps

The full Johnson Creek watershed is shown in Figure 6, and Figure 7 provides the optical-based shade model results. In general, forested areas have very high shading fraction, while heavily urbanized areas, agriculture and other cleared areas have very low shading fraction. Residential areas and other land cover types tend to have intermediate amounts of shade. Figures 8 and 9 illustrate the same area as Figures 2 and 3, corresponding to the white box in Figure 6. Both figures show the lidar-based shading fraction again. In Figure 8 the lidar-based shade is overlaid on half-meter satellite imagery, while in Figure 9 it is overlaid on the optical-based shade results. This allows easy identification of areas of disagreement between the lidar and optical models. The optical imagery-based shade results are available over the Johnson Creek watershed. The lidar-based shade results are available over the full three large pilot areas.

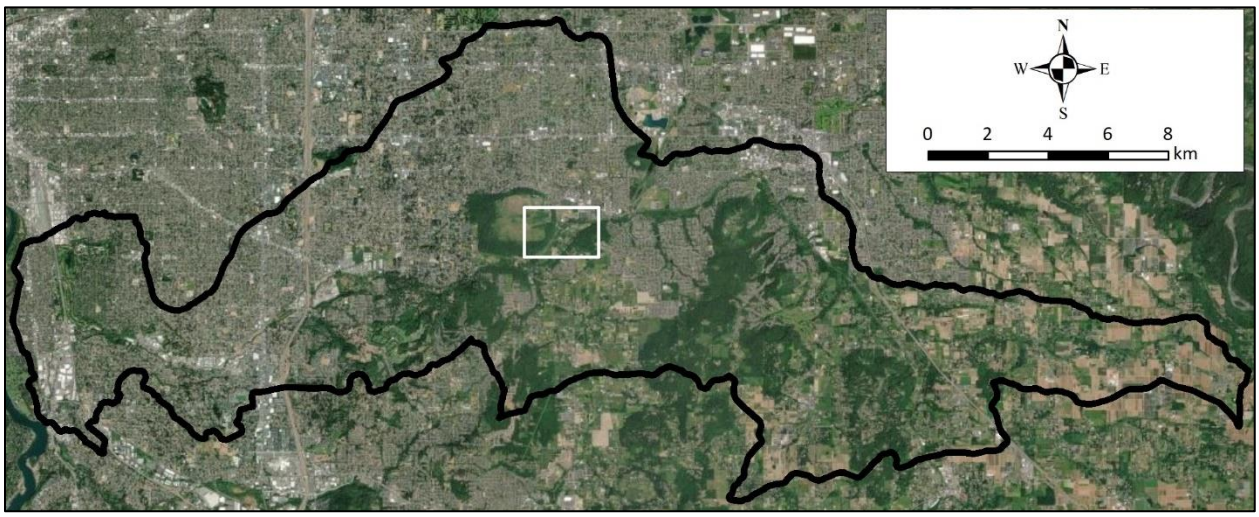

Figure 6. Johnson Creek watershed in southeast Portland, seen in summer 2021 0.5-meter commercial satellite imagery. The white box indicates the location of the zoomed view shown in Figures 2, 3, 8 and 9.

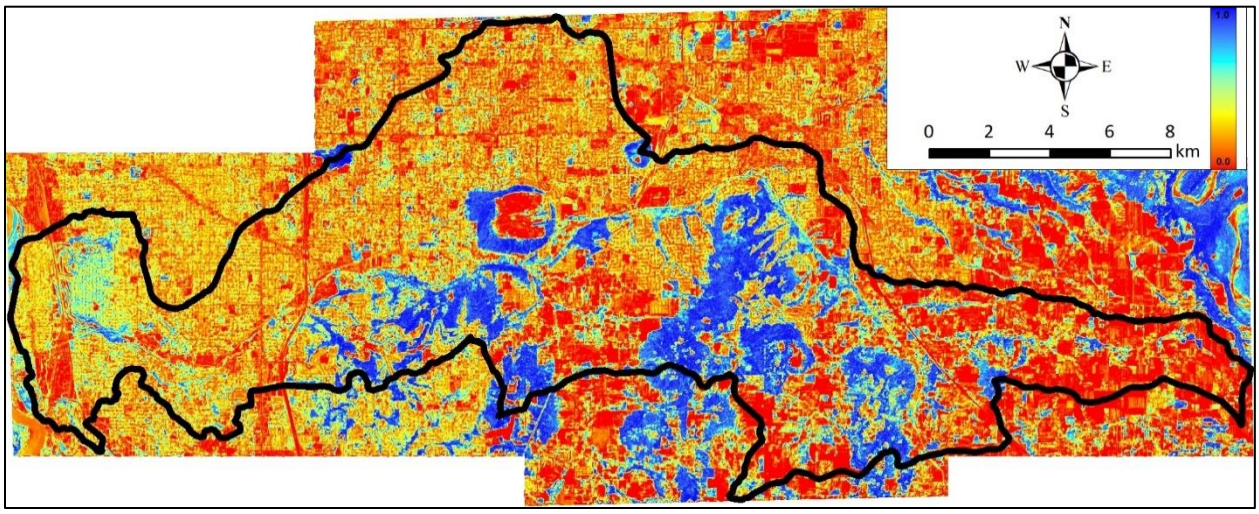

Figure 7. Optical imagery-based shading fraction for Johnson Creek watershed. Although the model was trained on riparian samples only, it was predicted everywhere. Results may be less reliable away from channels. Shading fraction is shown using the same color ramp as in Figures 2 and 3.

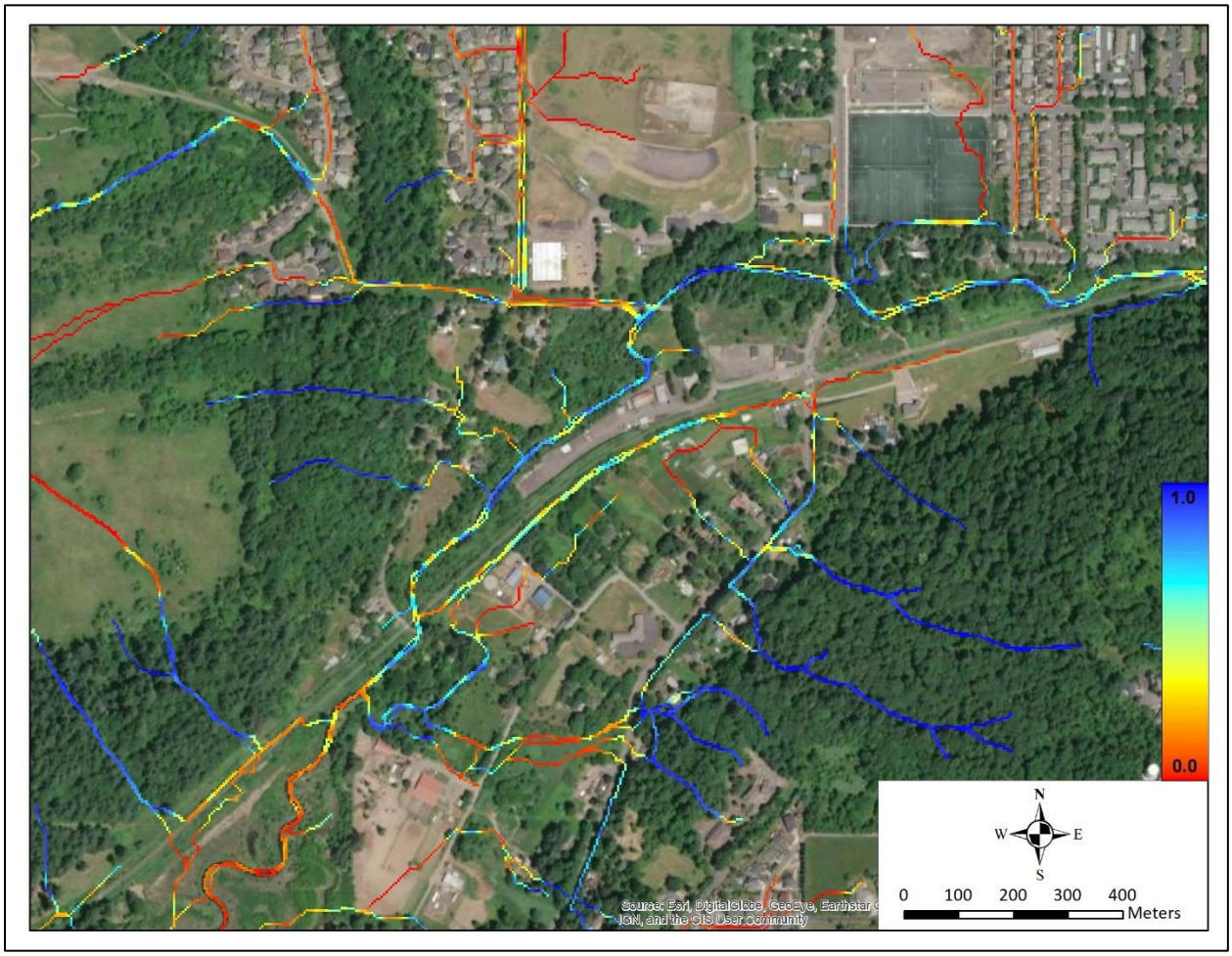

Figure 8. Shading fraction from lidar-based solar modeling, as in Figures 2 and 3, shown against 0.5-meter optical satellite imagery.

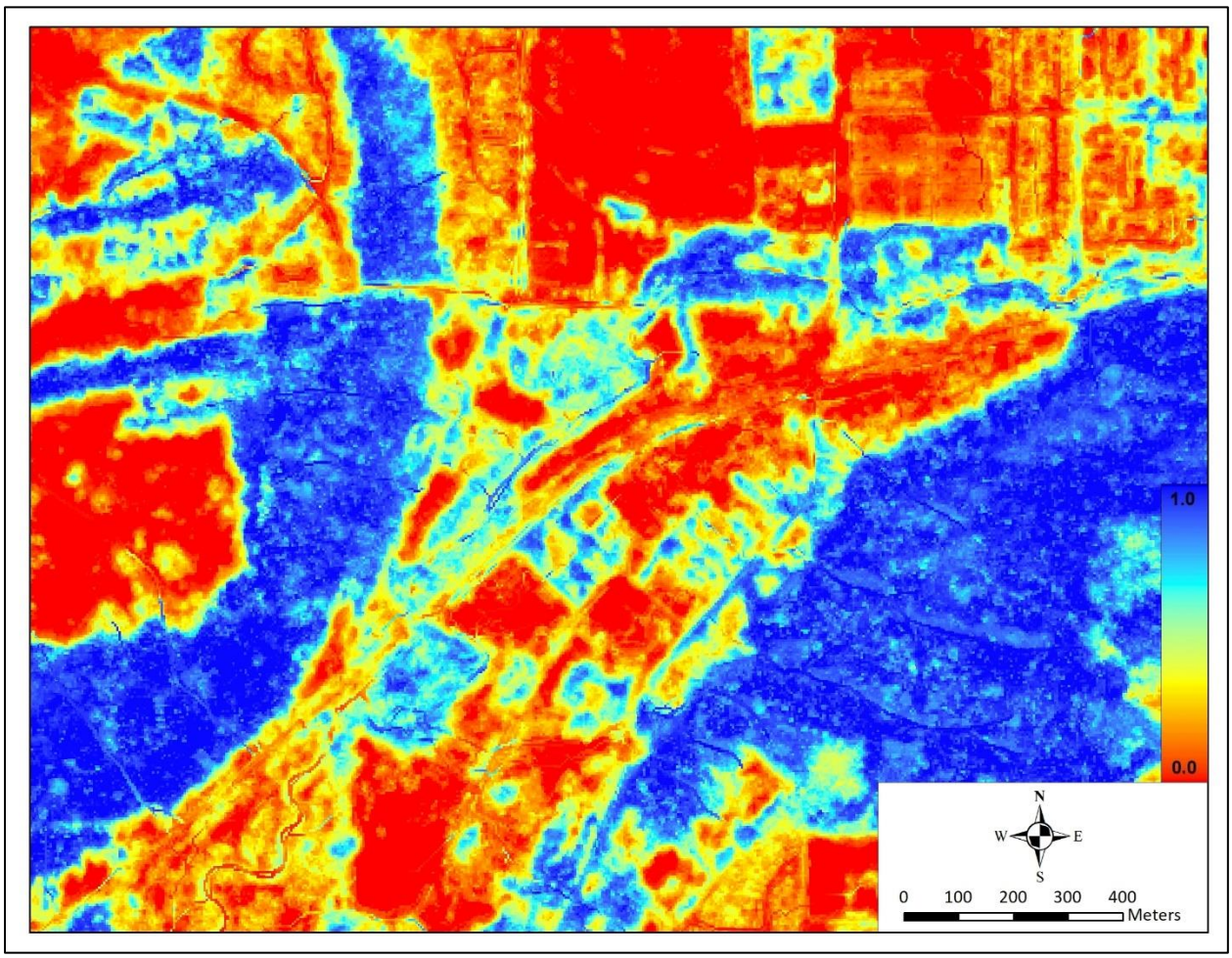

Figure 9. Lidar-based shading fraction superimposed on optical imagery-based shading fraction. The linear features from the lidar-based layer are only apparent where values disagree.

4. Discussion

Although we were not able to validate the lidar-based shade results due to the lack of field data. However, noting that they appeared to be quite accurate and matched expectations from imagery very well, we proceeded with validation of the optical-based shade model against the lidar-based results. The results of this validation indicate that effective shade on channels can be reliably mapped from inexpensive and regularly updated optical imagery, and that regular updating of riparian effective shade maps is achievable statewide for a very reasonable investment. Two unconventional techniques used to develop the predictor data—nested texture metrics (Nielsen and Noone 2014, Nielsen et al. 2021) and summarization of image metrics across a south-oriented window—were essential elements in achieving these promising results.

Optical imagery-based shade mapping could be used to prioritize watersheds for restoration, to help select "biggest bang for buck" restoration sites within watersheds, to assess the effectiveness of previous restoration efforts, and to provide an "effective shade dashboard" and assessments of improvement at reach, watershed, drainage basin, regional and statewide scales. Based on the results, we provide the following recommendations to ODEQ and other agencies and organizations committed to improving water quality and the health of riparian ecosystems in Oregon:

A. We strongly recommend that a current shade map be developed statewide or at least over high-priority TMDL watersheds. The currently available NAIP imagery could be used as a basis for

this—alternatively, new statewide imagery with similar specifications is being collected during Summer 2022.

B. We recommend that ODEQ proceed as soon as feasible with field sampling for two primary purposes. (1) Field sampling is needed to validate the lidar-based shade results with which the optical-based model was assessed. Based on manual comparison with imagery, there seems little doubt that the lidar results are accurate enough to use for this purpose, but it would be good to have the field results to ensure that loop is closed. (2) Field sampling would be helpful in determining other site-specific challenges that are not well-represented in lidar imagery which might affect optical mapping results under some circumstances. This information could be used to refine modeling methods in particular landscape types if desired in the future.

C. We recommend that impacts of the misregistration of NHD channels on effective shade mapping be evaluated. This could be accomplished as an office-based task for areas where lidar has been collected or in non-forest conditions, but would require fieldwork in forests without lidar coverage. The impacts are likely to vary by application. For example, applications requiring information summarized over large extents—such as prioritization of watersheds for restoration—may be little affected by NHD misregistration, as errors will likely balance out. But applications relying on site-specific information—such as identification of high priority restoration sites—may be greatly affected by misregistration. Once the impacts are known, attention should be given to assessing methods of enhancing or correcting the NHD in problem areas.

Acknowledgements

Funding was provided by a 319 Nonpoint Source Implementation Grant from the U.S. Environmental Protection Agency, administered by the Oregon Department of Environmental Quality as Agreement #095-21.

References

Belitz, K. and P.E. Stackelberg. 2021. Evaluation of six methods for correcting bias in estimates from ensemble tree machine learning regression models. Environmental Modelling & Software 139: 105006. Online: https://www.sciencedirect.com/science/article/pii/S1364815221000499.

ESRI. 2021. Modeling solar radiation. Online: https://desktop.arcgis.com/en/arcmap/latest/tools/spatial-analyst-toolbox/modeling-solar-radiation.htm.

Fox, E.W., R.A. Hill, S.G. Leibowitz, A.R. Olsen, D.J. Thornbrugh and M.H. Weber. 2017. Assessing the accuracy and stability of variable selection methods for random forest modeling in ecology. Environmental Monitoring and Assessment 189: 316. Online: https://doi.org/10.1007/s10661-017-6025-0.

Google. 2021. Google Earth Engine. Online: https://earthengine.google.com.

Liaw, A. and M. Wiener. 2002. Classification and regression by randomForest. R News 2002:18–22. Online: https://cran.r-project.org/doc/Rnews/Rnews_2002-3.pdf. Code available at: https://cran.r-project.org/package=randomForest.

National Renewable Energy Laboratory. 2015. Evaluation of the Aurora application shade measurement accuracy. NREL/FS-7A40-65558. Online: https://cdn2.hubspot.net/hubfs/3858309/AuroraSolarBlog_October2017/Docs/nrel-shading.pdf.

Nielsen, E.M., C. Copass, R.L. Brunner and L.K. Wise. 2021. Olympic National Park vegetation classification and mapping project report. Natural Resource Report NPS/NCCN/NRR—2021/2255. National Park Service, Fort Collins, Colorado. Online: https://irma.nps.gov/DataStore/Reference/Profile/2286420.

Nielsen, E.M. and M.D. Noone. 2014. Tree cover mapping for assessing greater sage-grouse habitat in eastern Oregon. Report, 10 pp. Portland, OR: Portland State University and The Nature Conservancy.

Oregon Department of Geology & Mineral Industries. 2021. DOGAMI lidar. Online: https://www.oregongeology.org/lidar.

Oregon Geospatial Enterprise Office. 2021. Imagery FIT. Online: https://www.oregon.gov/geo/Pages/imageryframe.aspx.

PRISM Climate Group. 2021. PRISM climate data. Online: https://prism.oregonstate.edu.

Zhang, G. and Y. Lu. 2011. Bias-corrected random forests in regression. Journal of Applied Statistics 39: 151-160. Online: http://dx.doi.org/10.1080/02664763.2011.578621.

Appendix A. Accessibility mask representativeness

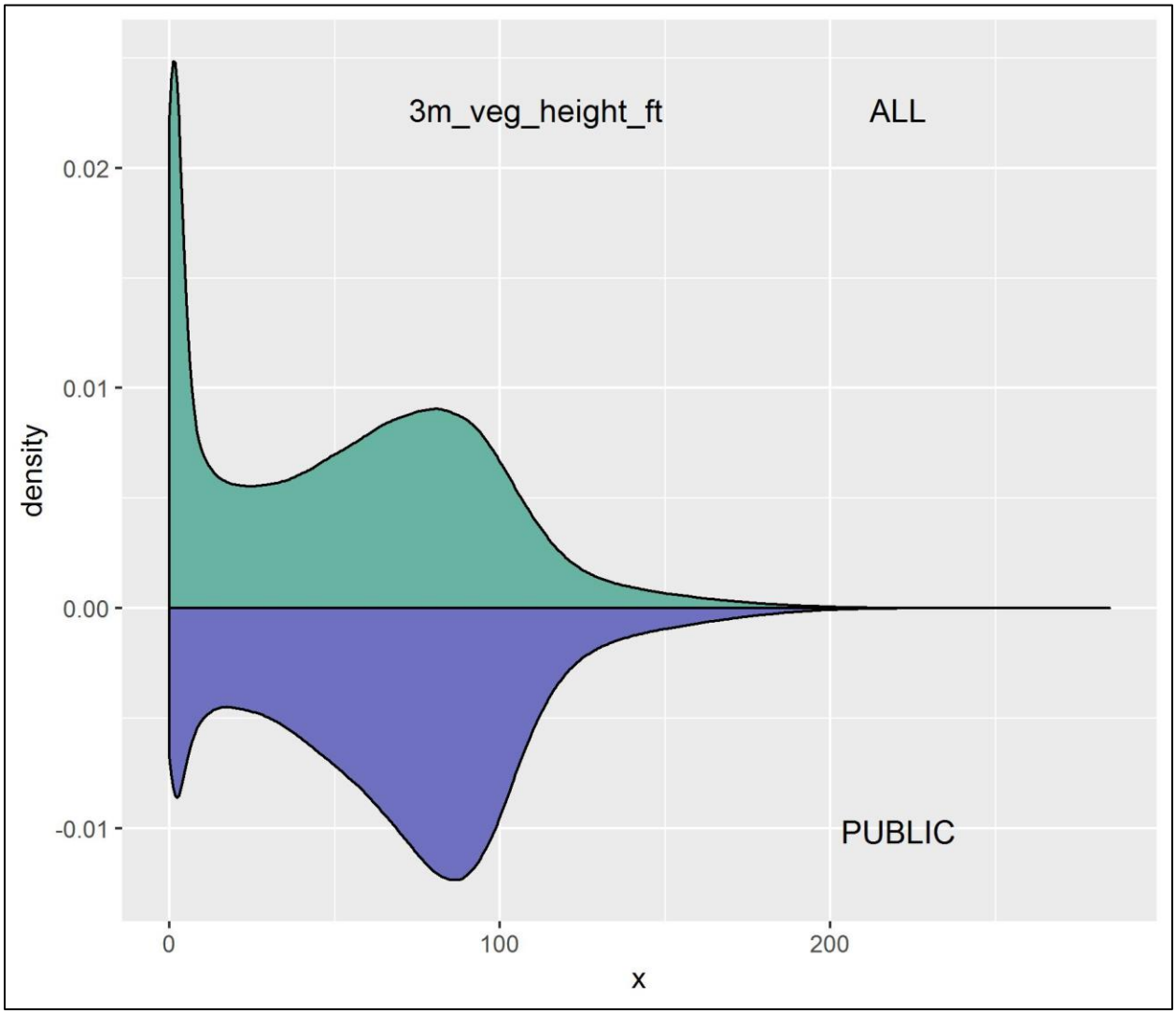

Figure 1a. Probability density function of vegetation height (in feet) within 20 meters of channels over all land in the sample watersheds vs. only over public lands.

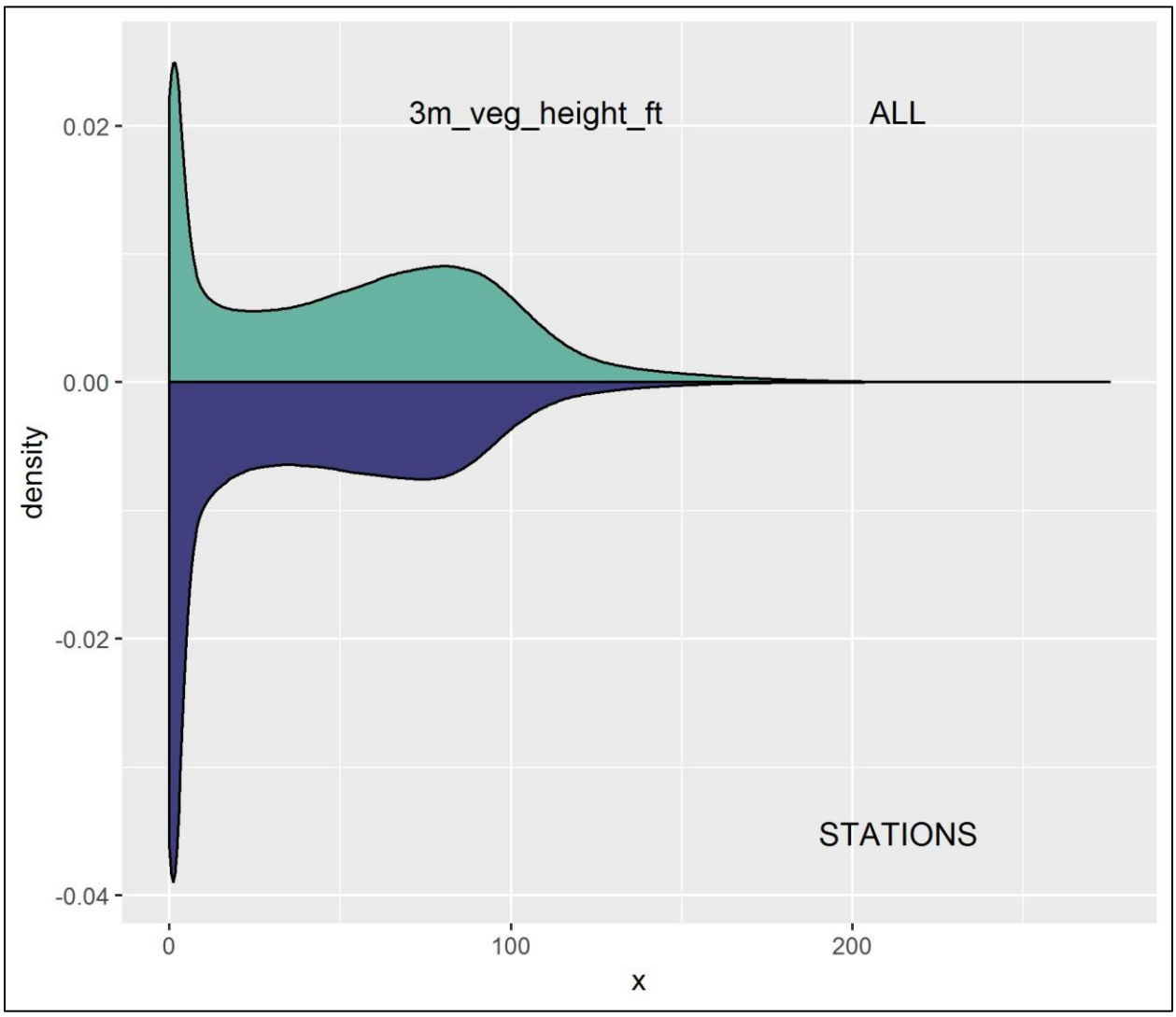

Figure 1b. Probability density function of vegetation height (in feet) within 20 meters of channels over all land in the sample watersheds vs. only within 100 meters of sample stations.

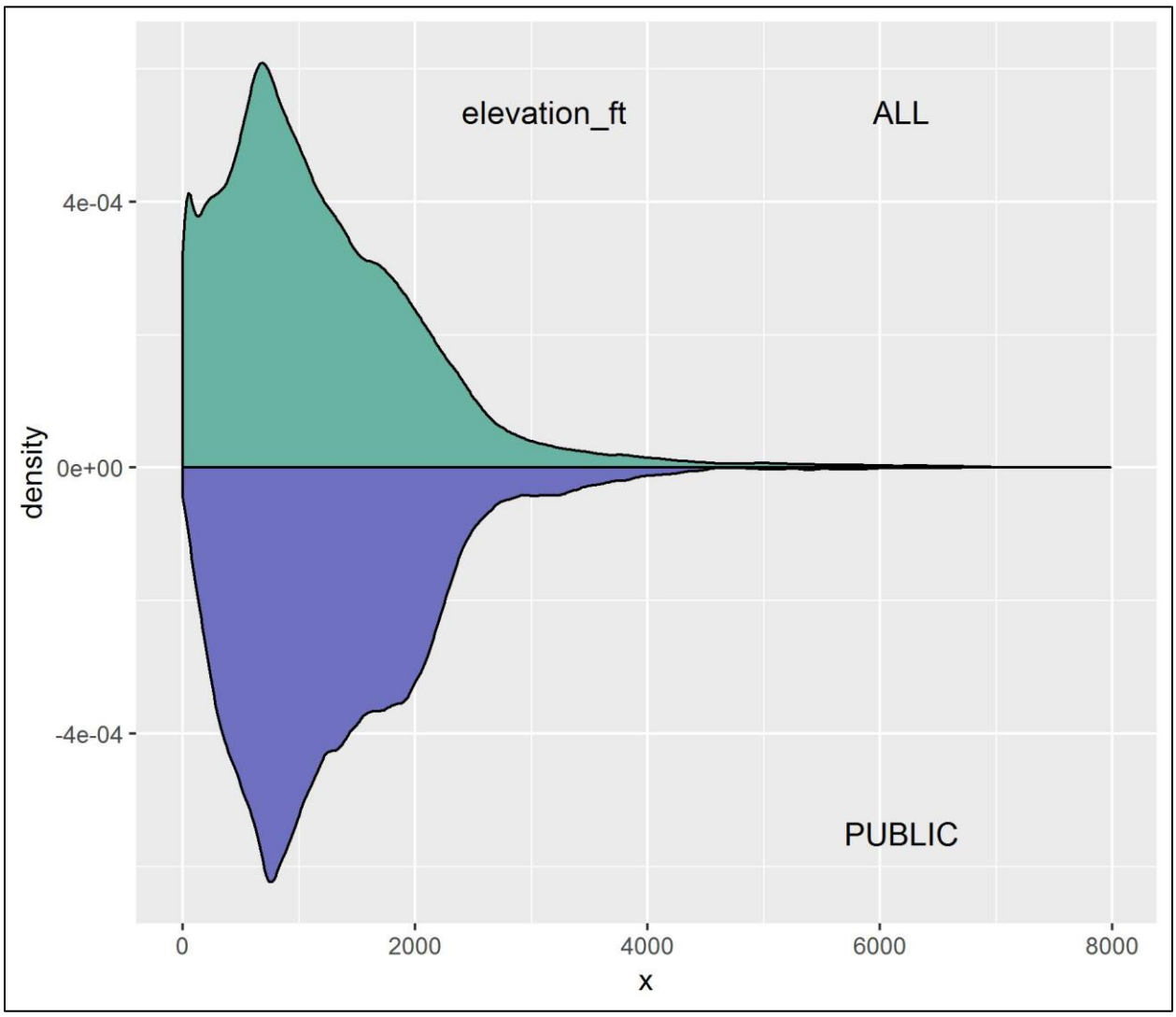

Figure 2a. Probability density function of elevation (in feet) within 20 meters of channels over all land in the sample watersheds vs. only over public lands.

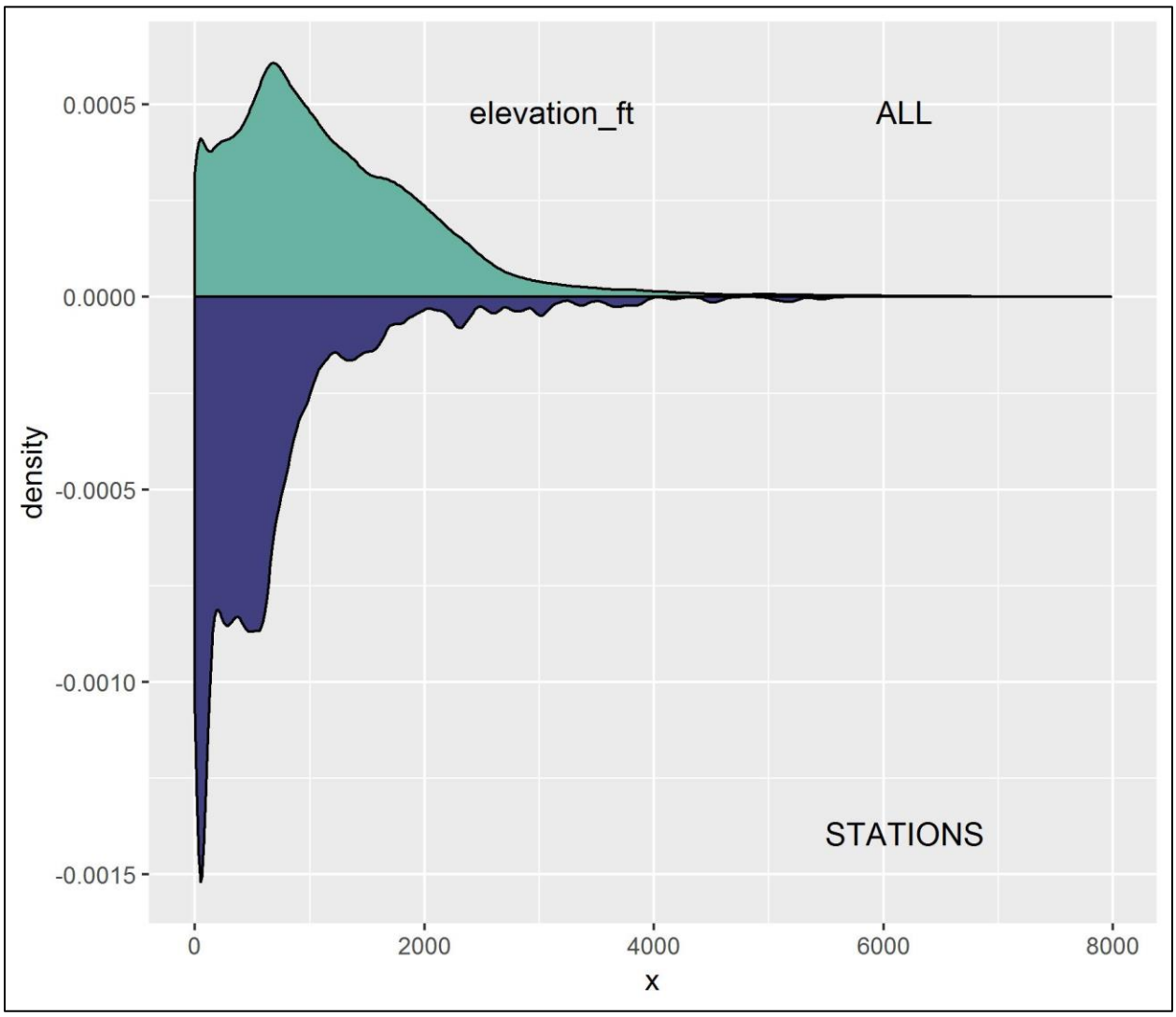

Figure 2b. Probability density function of elevation (in feet) within 20 meters of channels over all land in the sample watersheds vs. only within 100 meters of sample stations.

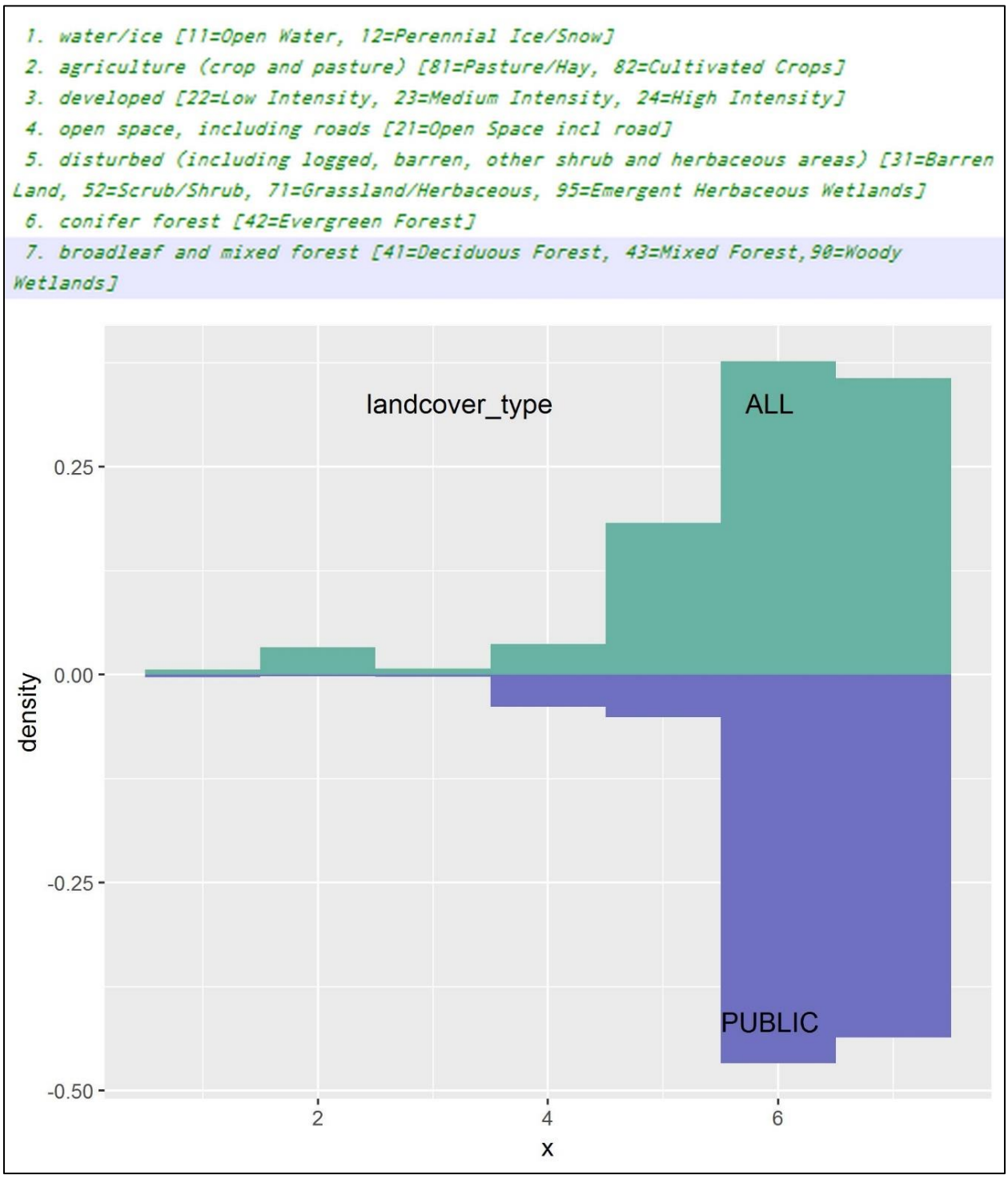

Figure 3a. Probability density function of seven lumped NLCD land cover types within 20 meters of channels over all land in the sample watersheds vs. only over public lands.

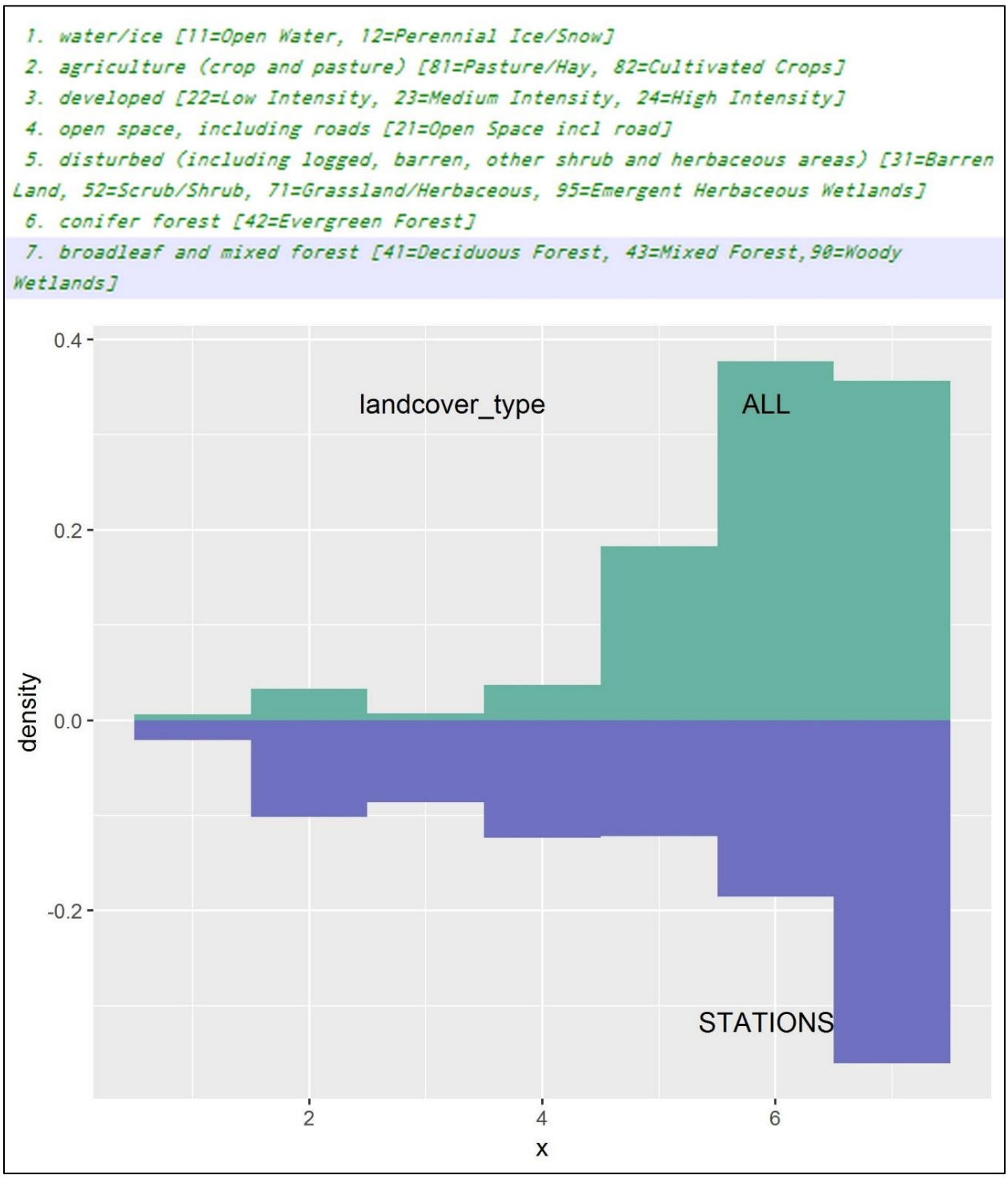

Figure 3b. Probability density function of seven lumped NLCD land cover types within 20 meters of channels over all land in the sample watersheds vs. only within 100 meters of sample stations.

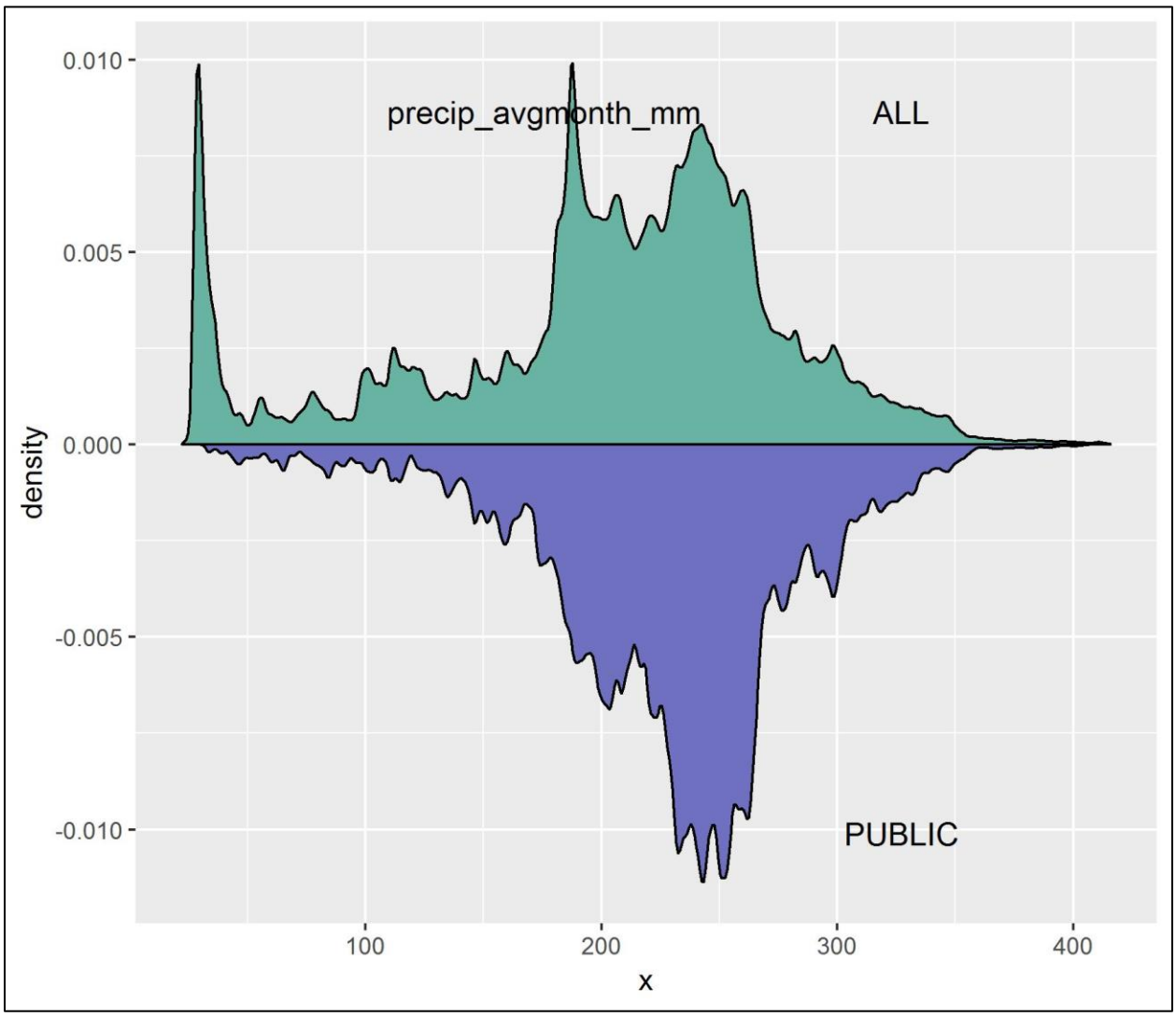

Figure 4a. Probability density function of average precipitation of January, April, July and October (in mm) within 20 meters of channels over all land in the sample watersheds vs. only over public lands.

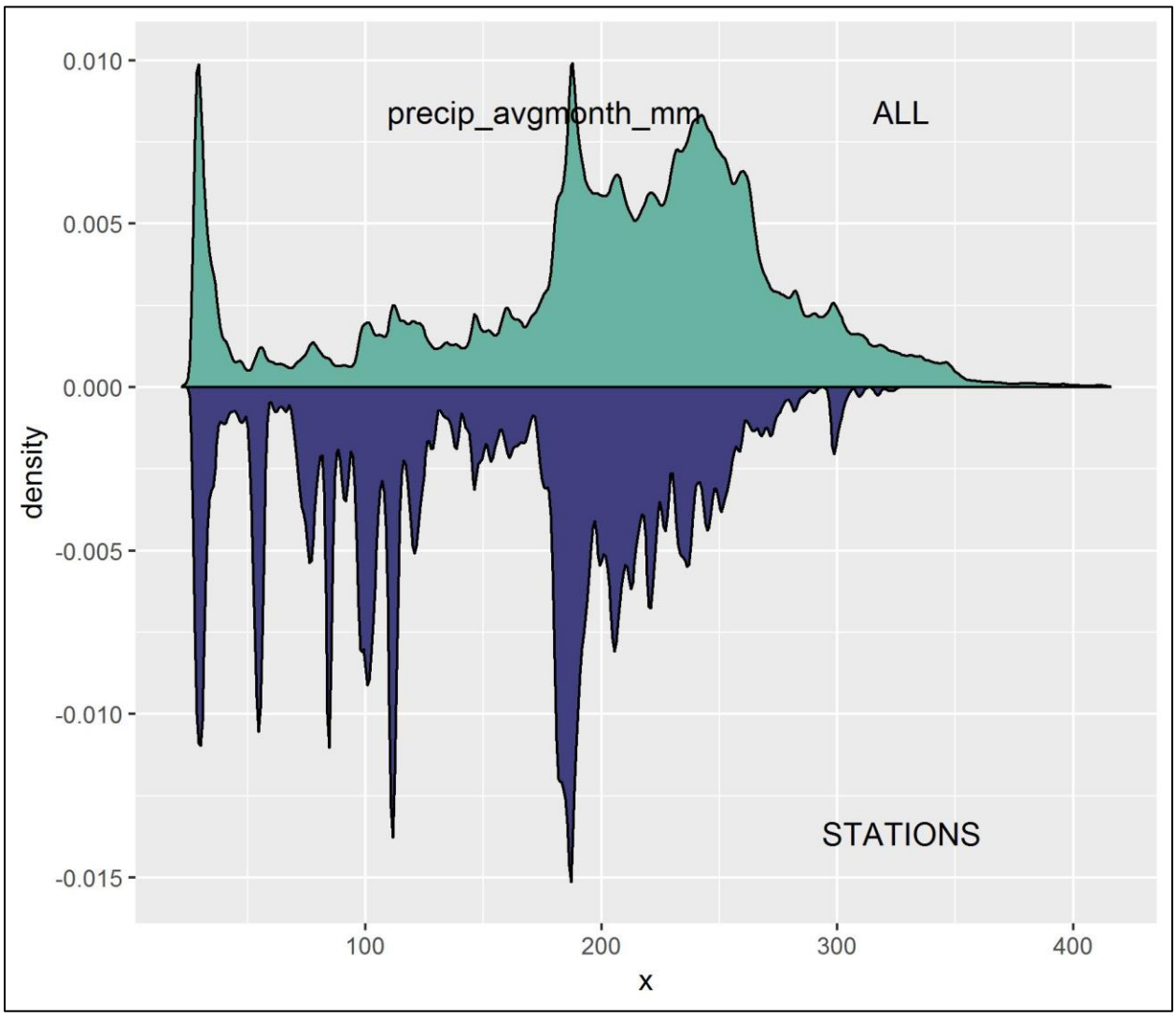

Figure 4b. Probability density function of average precipitation of January, April, July and October (in mm) within 20 meters of channels over all land in the sample watersheds vs. only within 100 meters of sample stations.

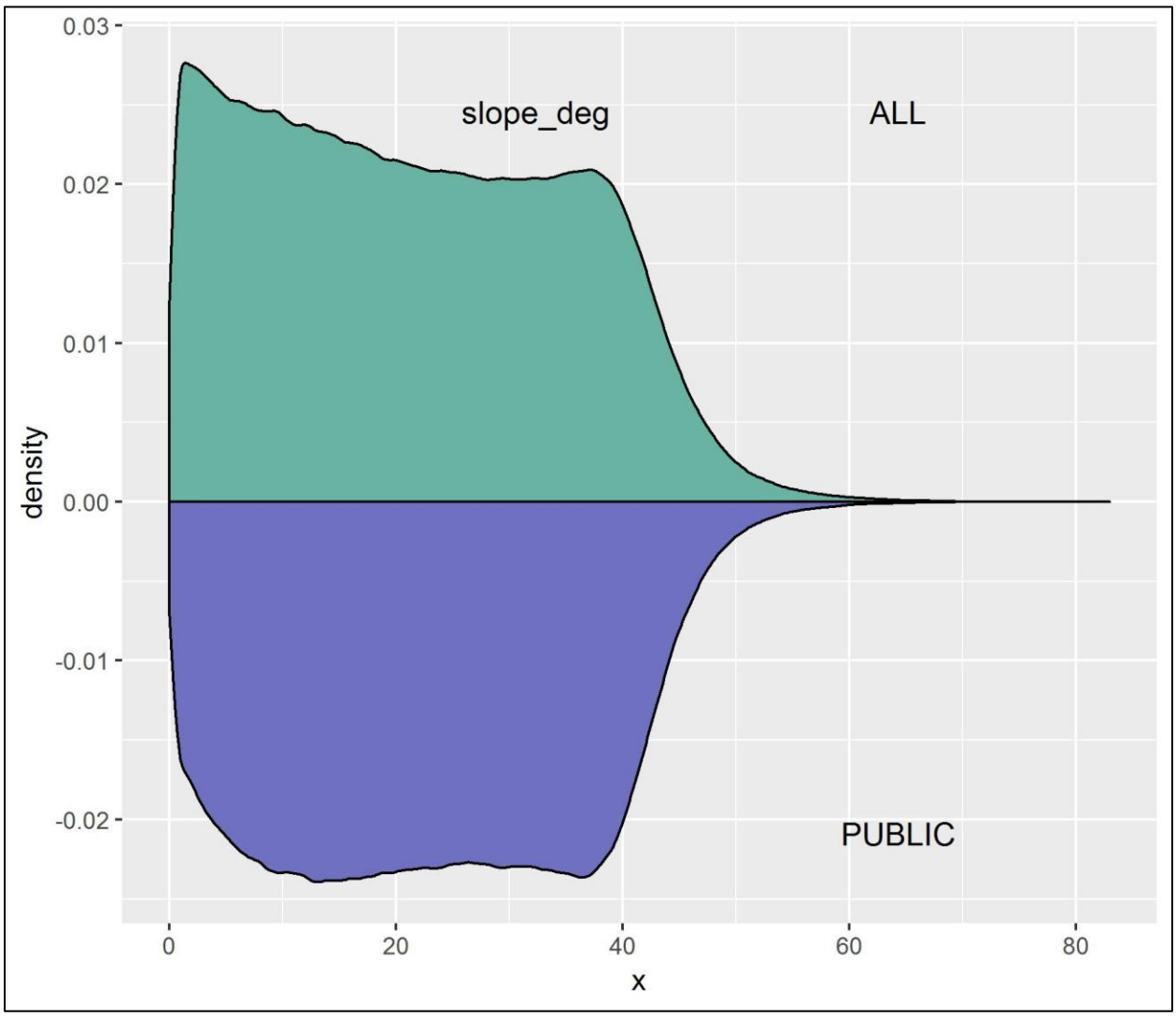

Figure 5a. Probability density function of slope (in degrees) within 20 meters of channels over all land in the sample watersheds vs. only over public lands.

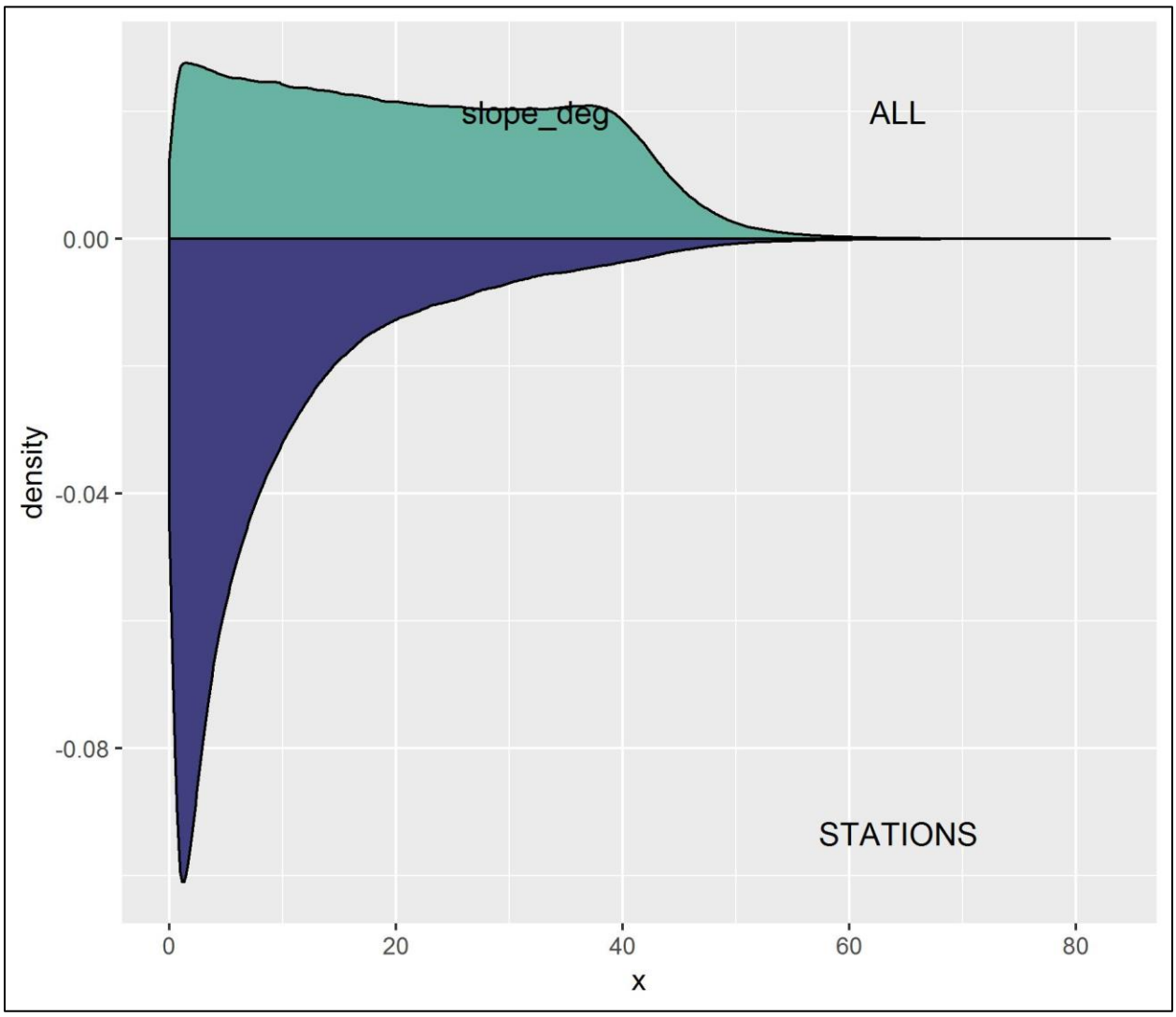

Figure 5b. Probability density function of slope (in degrees) within 20 meters of channels over all land in the sample watersheds vs. only within 100 meters of sample stations.

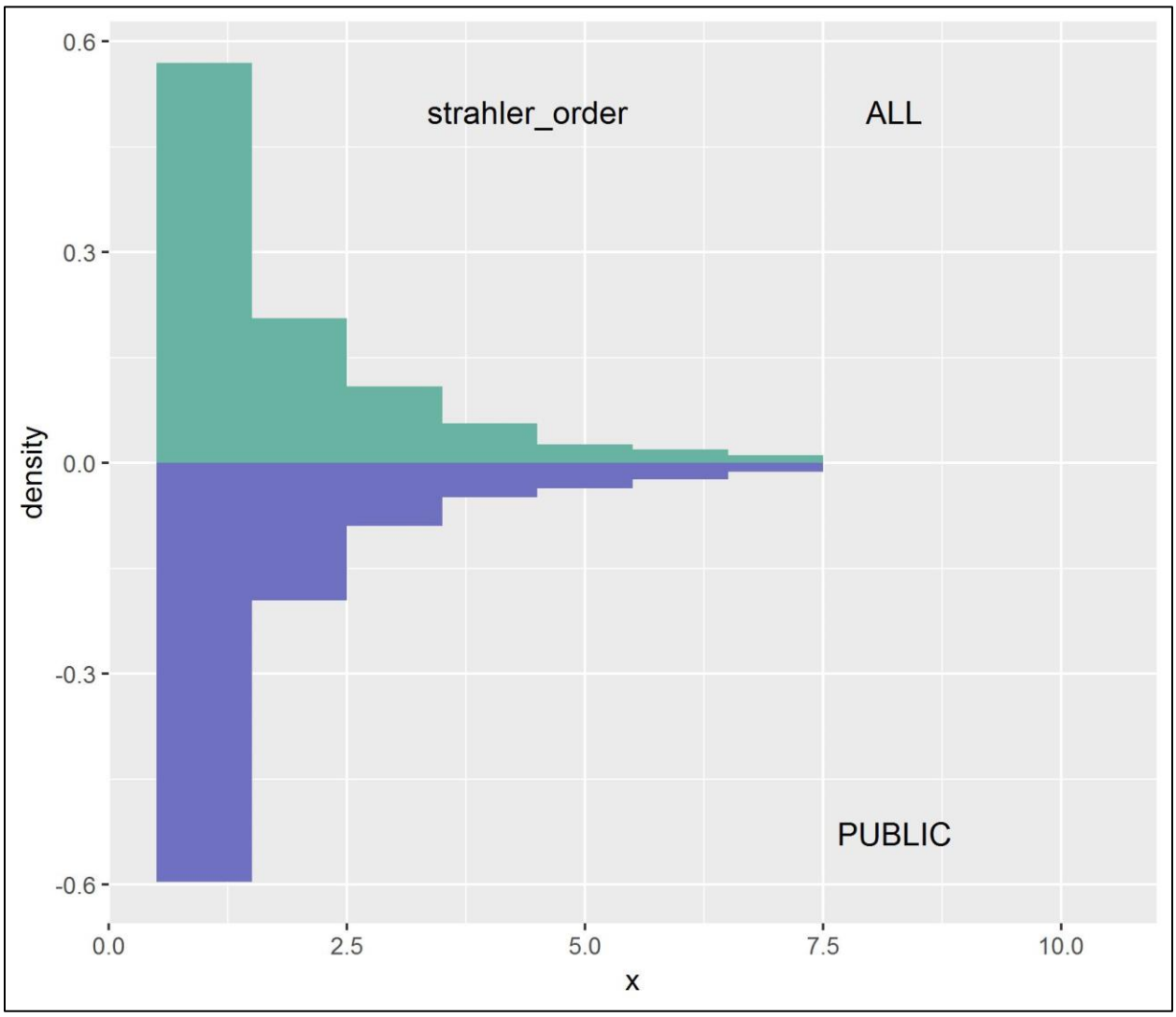

Figure 6a. Probability density function of Strahler stream order within 20 meters of channels over all land in the sample watersheds vs. only over public lands.

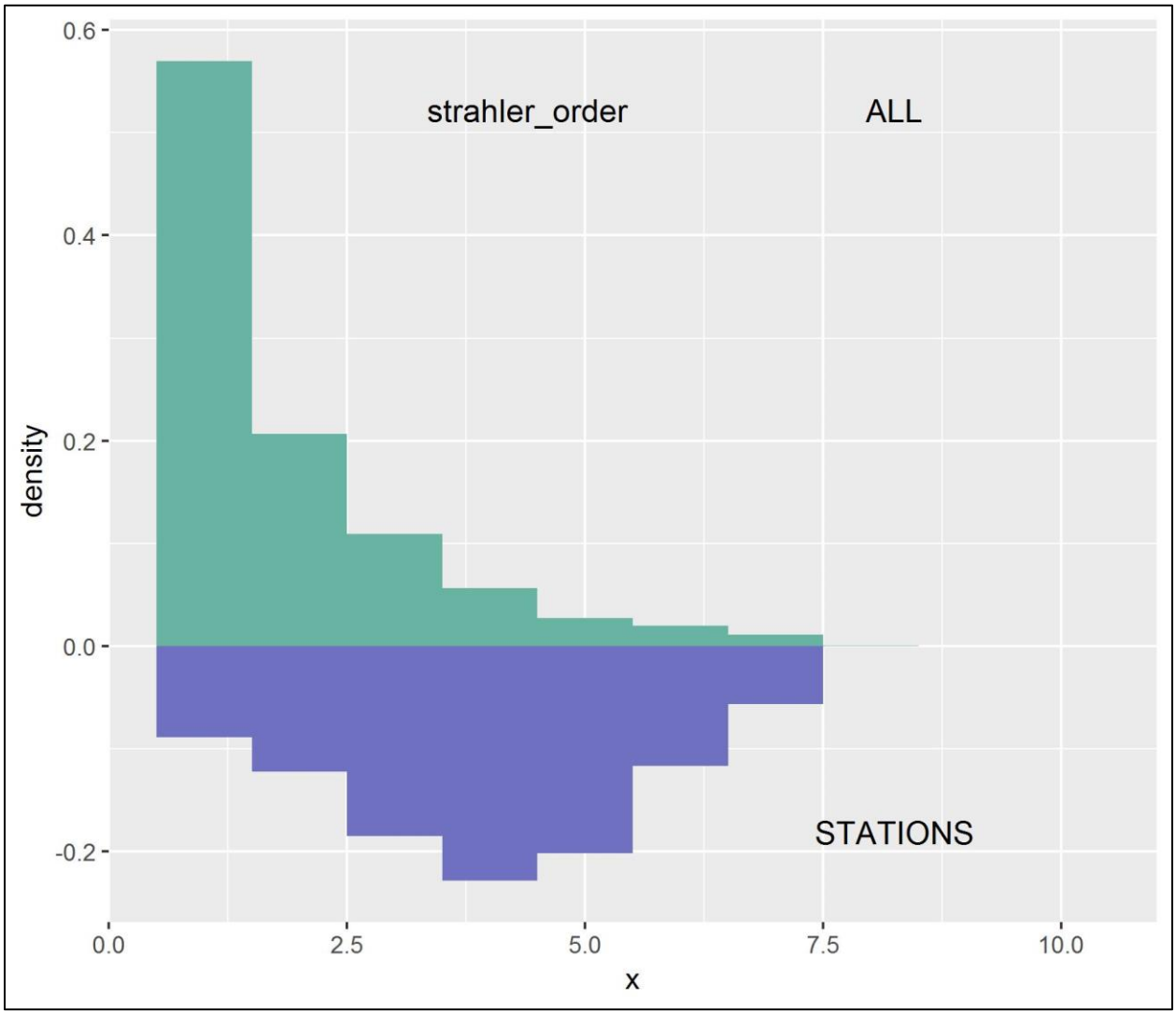

Figure 6b. Probability density function of Strahler stream order within 20 meters of channels over all land in the sample watersheds vs. only within 100 meters of sample stations.

Appendix B. Field sheet

SHADE 2021	Plot ID:	Date:	Observers:	Bank full width: m	Stream flow direction: deg
GPS unit:	Acc: m	UTM E:	N:	(Bank 1=HPP) Slope: deg Asp: deg	(Bank 2=opp) Slope: deg Asp: deg

Strata Codes

C1: conifers < 5'	B2: broadleaf tree 5-20'	H: vascular herbaceous
C2: conifers 5-20'	B3: broadleaf tree 20-80'	A: aquatic vegetation
C3: conifers 20-80'	B4: broadleaf tree 80'+	U: unvegetated
C4: conifers 80'+	S1: shrubs < 5'	W: water
B1: broadleaf tree < 5'	S2: shrubs 5-20'	I: intermittently flooded

VEGETATION COVER

Patch	Strata Code	Strata Ht	Veg Cover	Dominant Species
[A] Patch Diagram				
		ft	%	
		ft	%	
		ft	%	
		ft	%	
		ft	%	
		ft	%	
		ft	%	
		ft	%	
		ft	%	
		ft	%	
		ft	%	
		ft	%	
		ft	%	
		ft	%	
		ft	%	
		ft	%	
		ft	%	
		ft	%	
		ft	%	
		ft	%	
		ft	%	
		ft	%	
		ft	%	
		ft	%	
[B] Overlapping Channel				
		ft	%	
		ft	%	
		ft	%	
		ft	%	
		ft	%	
		ft	%	

Vegetation Cover Instructions

[A] Document strata for each patch in semi-circle. For each patch, begin with uppermost strata and record lower layers until reaching cumulative total 75%+ cover. For each strata estimate height and canopy cover. [B] Document strata that vertically overlap a 20-meter wide band across channel starting at HPP, centered on solar pathfinder points.

Hemi Photo Pt (HPP)

Conventional Photos

N	
E	
S	
W	

Solar Pathfinder Pts

1 (HPP)	
2	
3	
4	
5	

REFERENCE DIAGRAM

- Center on hemi photo pt
- Label reference objects, give distance & azimuth
- Sketch channel, to scale
- Indicate flow direction
- Show solar pathfinder pts
- Sketch major veg transitions in area

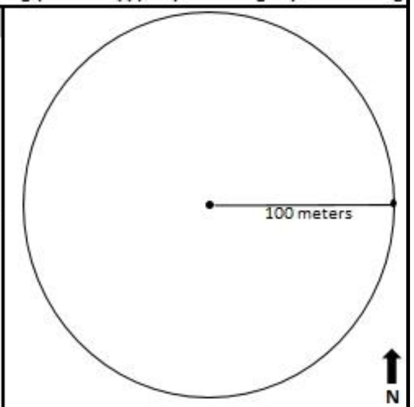

PATCH DIAGRAM

- Center on hemi photo pt
- Label veg patches of at least 25m2 (e.g., 5x5m)
- Describe patches, incl % of semicircle occupied
- Include unveg patches
- Label additional reference features

Patch A: ______ %,
Patch B: ______ %,
Patch C: ______ %,
Patch D: ______ %,
Patch E: ______ %,
Patch F: ______ %,

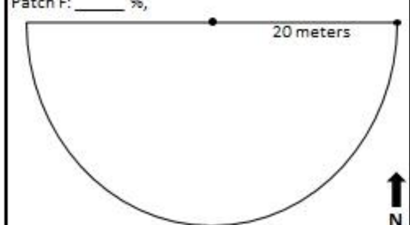

DESCRIPTION